Tran-SET

Transportation Consortium of South-Central States

*Solving Emerging Transportation Resiliency, Sustainability, and Economic Challenges through the Use of Innovative Materials and Construction Methods: From Research to Implementation*

# Bridge Deck Overlays Using Ultra-High Performance Concrete

**Project No. 17CNMS01**

**Lead University: New Mexico State University**

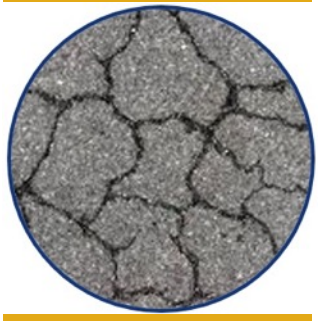

**Enhancing Durability and Service Life of Infrastructure**

**Final Report**

**October 2018**

**Disclaimer**

The contents of this report reflect the views of the authors, who are responsible for the facts and the accuracy of the information presented herein. This document is disseminated in the interest of information exchange. The report is funded, partially or entirely, by a grant from the U.S. Department of Transportation's University Transportation Centers Program. However, the U.S. Government assumes no liability for the contents or use thereof.

**Acknowledgments**

The authors would like to acknowledge the support and direction of the Project Review Committee that included Dr. Theresa Ahlborn of Michigan Technological University, Dr. Paul Barr of Utah State University, Dr. Narayanan Neithalath of Arizona State University, and Kathy Crowell of the New Mexico Department of Transportation.

# TECHNICAL DOCUMENTATION PAGE

| 1. **Project No.**<br>17CNMS01 | **2. Government Accession No.** | **3. Recipient's Catalog No.** |
|---|---|---|

| **4. Title and Subtitle**<br><br>Bridge Deck Overlays Using Ultra-High Performance Concrete | **5. Report Date**<br>Oct. 2018<br>**6. Performing Organization Code** |
|---|---|
| **7. Author(s)**<br>PI: Craig M. Newtson https://orcid.org/0000-0002-2140-9759<br>Co-PI: Brad D. Weldon https://orcid.org/0000-0001-7196-8690<br>GRA: Ahmed J. Al-Basha https://orcid.org/0000-0001-8192-8799<br>GRA: Mark P. Manning https://orcid.org/0000-0003-4862-7606<br>GRA: William K. Toledo https://orcid.org/0000-0002-3436-5118<br>GRA: Leticia D. Davila https://orcid.org/0000-0001-8608-189X | **8. Performing Organization Report No.** |
| **9. Performing Organization Name and Address**<br>Transportation Consortium of South-Central States (Tran-SET)<br>University Transportation Center for Region 6<br>3319 Patrick F. Taylor Hall, Louisiana State University<br>Baton Rouge, LA 70803 | **10. Work Unit No. (TRAIS)**<br><br>**11. Contract or Grant No.**<br>69A3551747106 |
| **12. Sponsoring Agency Name and Address**<br>United States of America<br>Department of Transportation<br>Research and Innovative Technology Administration | **13. Type of Report and Period Covered**<br>Final Research Report<br>May 2017 – May 2018<br>**14. Sponsoring Agency Code** |

**15. Supplementary Notes**
Report uploaded and accessible at: Tran-SET's website (http://transet.lsu.edu/)


**16. Abstract**

This study investigated the use of a locally produced ultra-high performance concrete (UHPC) as an alternative to typical overlay materials. Several bond strength tests including slant-shear, splitting tension, and direct tension tests were performed to assess the bond strength between UHPC and normal strength concrete (NSC) substrate with varying surface textures. Tests were also conducted to assess the early-age and longer-term shrinkage behavior and coefficient of thermal expansion of the UHPC as well as rapid chloride permeability testing. Good bond between UHPC and NSC substrate was observed even with inadequate surface texture.

Combined shrinkage and thermal effects were investigated for NSC slabs overlaid with the non-proprietary UHPC by analyzing five slab-overlay sections. Each slab-overlay had a single parameter varied to isolate the effects of thickness of the NSC substrate, substrate reinforcement ratio, and exposure conditions. Increased steel reinforcement and thickness of the NSC substrate were observed to reduce the effect of UHPC overlay shrinkage.

The final major experiment was to overlay a full-scale channel girder to assess the response of a high-performance concrete, pre-stressed bridge girder with a 1-in. (25-mm) UHPC overlay to flexural loading. The girder was subjected to 1000 load-unload cycles to specified service load conditions. Cyclic loading was applied both before and after application of the UHPC overlay to provide a comparison of global behavior and performance of the girder and overlay. Finally, the girder with overlay was loaded to failure to investigate post-cracking and ultimate behavior of the composite member. Little to no visible distress was observed in the overlay until loads were applied that were significantly greater than expected under normal service conditions.

The results indicated that the non-proprietary UHPC has the potential to serve as an overlay material as long as proper measures are used to prepare the substrate surface and ensure a high quality bond with the existing deck.


| **17. Key Words**<br>Overlay, Bridge Deck, Concrete , UHPC, Rehabilitation, Service Life | **18. Distribution Statement**<br>No restrictions. |
|---|---|

| **19. Security Classif. (of this report)** | **20. Security Classif. (of this page)** | **21. No. of Pages** | **22. Price** |
|---|---|---|---|
| Unclassified | Unclassified | 69 | |

**Form DOT F 1700.7 (8-72)** **Reproduction of completed page authorized.**

## SI* (MODERN METRIC) CONVERSION FACTORS

### APPROXIMATE CONVERSIONS TO SI UNITS

| Symbol | When You Know | Multiply By | To Find | Symbol |
|---|---|---|---|---|
| | | **LENGTH** | | |
| in | inches | 25.4 | millimeters | mm |
| ft | feet | 0.305 | meters | m |
| yd | yards | 0.914 | meters | m |
| mi | miles | 1.61 | kilometers | km |
| | | **AREA** | | |
| $in^2$ | square inches | 645.2 | square millimeters | $mm^2$ |
| $ft^2$ | square feet | 0.093 | square meters | $m^2$ |
| $yd^2$ | square yard | 0.836 | square meters | $m^2$ |
| ac | acres | 0.405 | hectares | ha |
| $mi^2$ | square miles | 2.59 | square kilometers | $km^2$ |
| | | **VOLUME** | | |
| fl oz | fluid ounces | 29.57 | milliliters | mL |
| gal | gallons | 3.785 | liters | L |
| $ft^3$ | cubic feet | 0.028 | cubic meters | $m^3$ |
| $yd^3$ | cubic yards | 0.765 | cubic meters | $m^3$ |
| | | NOTE: volumes greater than 1000 L shall be shown in $m^3$ | | |
| | | **MASS** | | |
| oz | ounces | 28.35 | grams | g |
| lb | pounds | 0.454 | kilograms | kg |
| T | short tons (2000 lb) | 0.907 | megagrams (or "metric ton") | Mg (or "t") |
| | | **TEMPERATURE (exact degrees)** | | |
| °F | Fahrenheit | 5 (F-32)/9<br>or (F-32)/1.8 | Celsius | °C |
| | | **ILLUMINATION** | | |
| fc | foot-candles | 10.76 | lux | lx |
| fl | foot-Lamberts | 3.426 | $candela/m^2$ | $cd/m^2$ |
| | | **FORCE and PRESSURE or STRESS** | | |
| lbf | poundforce | 4.45 | newtons | N |
| $lbf/in^2$ | poundforce per square inch | 6.89 | kilopascals | kPa |

### APPROXIMATE CONVERSIONS FROM SI UNITS

| Symbol | When You Know | Multiply By | To Find | Symbol |
|---|---|---|---|---|
| | | **LENGTH** | | |
| mm | millimeters | 0.039 | inches | in |
| m | meters | 3.28 | feet | ft |
| m | meters | 1.09 | yards | yd |
| km | kilometers | 0.621 | miles | mi |
| | | **AREA** | | |
| $mm^2$ | square millimeters | 0.0016 | square inches | $in^2$ |
| $m^2$ | square meters | 10.764 | square feet | $ft^2$ |
| $m^2$ | square meters | 1.195 | square yards | $yd^2$ |
| ha | hectares | 2.47 | acres | ac |
| $km^2$ | square kilometers | 0.386 | square miles | $mi^2$ |
| | | **VOLUME** | | |
| mL | milliliters | 0.034 | fluid ounces | fl oz |
| L | liters | 0.264 | gallons | gal |
| $m^3$ | cubic meters | 35.314 | cubic feet | $ft^3$ |
| $m^3$ | cubic meters | 1.307 | cubic yards | $yd^3$ |
| | | **MASS** | | |
| g | grams | 0.035 | ounces | oz |
| kg | kilograms | 2.202 | pounds | lb |
| Mg (or "t") | megagrams (or "metric ton") | 1.103 | short tons (2000 lb) | T |
| | | **TEMPERATURE (exact degrees)** | | |
| °C | Celsius | 1.8C+32 | Fahrenheit | °F |
| | | **ILLUMINATION** | | |
| lx | lux | 0.0929 | foot-candles | fc |
| $cd/m^2$ | $candela/m^2$ | 0.2919 | foot-Lamberts | fl |
| | | **FORCE and PRESSURE or STRESS** | | |
| N | newtons | 0.225 | poundforce | lbf |
| kPa | kilopascals | 0.145 | poundforce per square inch | $lbf/in^2$ |

# TABLE OF CONTENTS

## LIST OF FIGURES

## LIST OF TABLES

## ACRONYMS, ABBREVIATIONS, AND SYMBOLS

| | |
|---|---|
| AASHTO | American Association of State Highway and Transportation Officials |
| AE | Acoustic emissions |
| BS | British Standard |
| CL | Cyclic loading |
| HPC | High performance concrete |
| LMC | Latex-modified concrete |
| LRFD | Load and resistance factor design |
| LSC | Low slump concrete |
| LVDT | Linearly variable displacement transducers |
| NMDOT | New Mexico Department of Transportation |
| NMSU | New Mexico State University |
| NSC | Normal strength concrete |
| PBC | Polymer-based concrete |
| RCPT | Rapid chloride permeability test |
| SCM | Supplementary cementitious material |
| SG | Strain gauge |
| SSMTL | Structural Systems and Materials Testing Laboratory |
| Tran-SET | Transportation Consortium of South-Central States |
| TXDOT | Texas Department of Transportation |
| UHPC | Ultra-high performance concrete |
| VWSG | Vibrating wire strain gauge |

## EXECUTIVE SUMMARY

The work presented in this report investigates the use of locally produced ultra-high performance concrete (UHPC) as an alternative to typical overlay materials. Several bond strength tests including slant-shear, splitting tension, and direct tension tests were performed to assess the bond strength between UHPC and normal strength concrete (NSC) substrate with varying surface textures. Four surface textures were investigated that included lightly ground, horizontal, cross-hatched, and rough with texture depths 0.002, 0.035, 0.063, and 0.11 in. (0.05, 0.9, 1.6, and 2.8 mm), respectively. ACI recommends a minimum slant-shear bond strength of 1000 psi (7 MPa) and a minimum tensile bond strength of 150 psi (1 MPa) for repair concrete. It was concluded from the bond strength tests that development of a proper bond between UHPC and NSC can be achieved without the use of bonding agents. However, bond strength is highly dependent on the texture of the substrate material. Desirable bond strength from slant-shear and splitting tension specimens was achieved even in the case of inadequate texturing (lightly ground texture). Acceptable direct tensile strengths were achieved only with chipped textures, which can cause worse damage to the substrate than other surface preparation methods expected in the field. Most importantly, the minimum acceptable texture depth under field conditions is 0.25 in. (6.35 mm). Since all of the bond assessment tests were able to produce adequate bond strengths with textures less than 0.08 in. (2 mm), the results are particularly attractive.

Tests to assess the early-age and longer-term shrinkage behavior and coefficient of thermal expansion of the UHPC were also performed to understand how these properties might affect the overlay performance. Additionally, rapid chloride permeability testing was conducted to assess the ability of the UHPC to resist chloride ion penetration. The results of this study indicate that locally produced UHPC seems to have the potential to serve as an overlay material as long as proper measures are used in texturing the substrate to ensure that proper bond is achieved.

Combined shrinkage and thermal effects were investigated for NSC slabs overlaid with UHPC through the analysis of five slab-overlay sections. Each slab had a reinforcement mesh consisting of six bars, three in each direction. Also, each slab-overlay had a single parameter variation to isolate and investigate the effect of different design parameters. Parameter variations included thickness of the NSC substrate, substrate reinforcement steel area, overlay application, and exposure conditions. The slabs were all textured with handheld air hammers to depths ranging from 0.054 in. (1.37 mm) to 0.153 in. (3.89 mm). Strains in each substrate were measured with vibrating wire strain gauges to identify the influence that shrinkage of the UHPC overlay had on the substrate. Shrinkage effects of the UHPC overlay were isolated to identify key design factors that influence behavior. It was observed that increased steel reinforcement and increased thickness of the NSC substrate reduced the effect of the UHPC overlay shrinkage. Neutral axis location was also monitored in the slab-overlay specimens. As expected, slabs experienced less shrinkage when more reinforcing steel was provided. Thicker slabs also experienced greater shrinkage than thinner slabs. Slabs that were kept in a controlled environment (laboratory) experienced more uniform shrinkage over time, as expected.

The final major experiment in this research was to overlay a 25-foot (7.62-m) channel girder to assess the effects of the overlay on mechanical performance during cyclic loading. The research

investigated the behavioral response of a full-scale, high-performance concrete (9.5 ksi [66 MPa]) pre-stressed bridge girder with a 1-in. (25-mm) UHPC overlay to longitudinal four-point flexural loading. The overlay was cast using a nonproprietary UHPC mixture consisting primarily of local materials and high-strength steel fiber reinforcement. The girder was subjected to cyclic, longitudinal four-point flexural loading consisting of a minimum of 1000 load-unload cycles to specified service load conditions. Cyclic loading was applied both before and after the placement of the UHPC overlay to provide comparative analyses of global behavior and performance of the girder and overlay. Finally, the girder with overlay was loaded in longitudinal four-point flexure to failure conditions to investigate post-cracking and ultimate behavior of the composite member. Cyclic load testing of the overlaid girder concluded that there was a clear increase in flexural stiffness after addition of the UHPC overlay. The flexural behavior exhibited by the girder with a UHPC overlay during ultimate loading provided further confidence in the performance of non-proprietary UHPC for overlay applications. Behavior during deflection increment cyclic loadings provided evidence that the composite section maintained elastic behavior prior to cracking. Final ultimate loading also demonstrated the performance of the UHPC overlay. Even with high concentrations of flexural and flexural-shear cracking in and around the pure-moment region, many extending up to deck level, little to no cracking, crushing, or other visible distress was observed on the UHPC overlay. The only distress observed that was related to the overlay was isolated delamination that occurred at significantly greater loads than expected under normal service conditions.

Recommendations that can be made from the results of this study include:

1. Bonding agents should not be used to bond UHPC overlay to the substrate material because nano-scale particles in UHPC provide sufficient bond for marginally textured surfaces as long as they are clean and saturated prior to application of the overlay.
2. Although much of the laboratory work in this research used grinding for surface preparation and texturing, it is not an acceptable practice in the field. Preferred surface preparation methods are shot blasting or hydro-demolition because they do not cause microcracks in the substrate.
3. Care should be taken to ensure that the UHPC mixture has adequate workability to facilitate the installation process. Additionally, steel screeds and tools are preferable to lumber. Desirable finishing methods should be able to be performed before the formation of drying shrinkage cracks.

## IMPLEMENTATION STATEMENT

During the implementation phase of this project (May 8, 2018 through November 7, 2018), design recommendations are to be documented that may be used by state departments of transportation for field implementation of bridge deck overlays using UHPC produced with local materials. The document that conveys the design recommendations will be submitted at the end of the implementation phase (November 2018). Although it was hoped that the New Mexico Department of Transportation (NMDOT) would be able to identify a suitable bridge deck overlay project for field implementation of this research during the project period, the timing of such a project could not be assured. Therefore, the production and dissemination of these recommendations were defined in the project contract to constitute implementation of the research.

At this time, the NMDOT does plan to implement the research findings on a bridge deck overlay project in 2019. A follow-up research project is planned to monitor and document the construction and performance of that UHPC overlay.

Education, outreach, technology transfer, and workforce development activities for this project are also considered to be implementation activities. As part of these activities, one of the expected deliverables is a PowerPoint presentation to facilitate educational outreach opportunities in schools and for the general public. Development of the PowerPoint presentation containing the educational content will target education and recruitment of high school and community college students that are considering transportation engineering careers, interested in construction-related careers, or are interested in pursuing careers in the concrete industry. The PowerPoint file will be made available through Tran-SET.

Other outreach and technology activities include presentation of the research at conferences, meetings, and workshops associated with Tran-SET and the transportation engineering community. Presentation of the research has occurred, or is planned to occur, in the following forms and conferences:

1. Presentation and abstract, "Bridge Deck Overlays using Ultra-High Performance Concrete," presented at the 2018 Tran-SET First Annual Conference, New Orleans.
2. Poster by William K. Toledo, "Bridge Deck Overlays using Ultra-High Performance Concrete," presented at the 2018 Tran-SET Annual Conference, New Orleans.
3. Poster by William K. Toledo, "Bridge Deck Overlays using Ultra-High Performance Concrete," presented at TransCon, Las Cruces, April 18-20, 2018.
4. Presentation by Craig Newtson, "Bridge Deck Overlays using Ultra-High Performance Concrete," presented at TransCon, Las Cruces, April 18-20, 2018.
5. Conference paper, "Ultra-High Performance Concrete Overlays for Concrete Bridge Decks," presented at 3rd World Multidisciplinary Civil Engineering, Architecture, and Urban Planning Symposium, Prague, June 18-22, 2018.
6. Presentation by Craig Newtson, "Ultra-High Performance Concrete Overlays for Concrete Bridge Decks," presented at 3rd World Multidisciplinary Civil Engineering, Architecture, and Urban Planning Symposium, Prague, June 18-22, 2018.

7. Conference paper submitted to the 2019 Transportation Research Board conference in Washington, DC, "Behavioral Study of Ultra-High Performance Concrete (UHPC) using Local Materials as an Overlay."
8. Conference paper submitted to the 2019 Transportation Research Board conference in Washington, DC, "Flexural Testing and Behavior of Prestressed Channel Girder and Locally Produced Ultra-High Performance Concrete Overlay."
9. Conference paper and poster will be submitted for the 2019 Tran-SET Conference.

# 1. INTRODUCTION

## 1.1. Background

A major issue facing the world's infrastructure is rapidly degrading concrete bridge decks. Concrete bridge decks can be exposed to a wide range of environmental and mechanical distress types and are critical bridge elements since they not only provide a comfortable and safe riding surface but also protect structural elements beneath them. According to 2016 United States National Bridge Inventory data, 23.9% of US bridges have concrete bridge decks in "Satisfactory" condition and only 10 out of 43 transportation agencies anticipate that their bridge deck overlays have service lives greater than 25 years *(1)*.

Bridge deck maintenance is expensive because of harsh exposure that shortens anticipated service life. The high cost of maintenance has led agencies to consider more durable materials for use as bridge deck overlays. A wide range of materials are currently available for overlaying applications including asphalt concrete, high performance concrete, low-slump concrete, latex-modified concrete, and polymer-modified concrete. However, each of these materials has drawbacks such as high cost, inadequate service life expectancy, or limited availability.

This study focuses on assessing the possibility of using ultra-high performance concrete (UHPC) produced with local materials to overlay existing concrete bridge decks. UHPC's exceptional mechanical and durability properties *(1-4)* provide the potential to greatly improve the service life of existing bridge decks and their durability. The use of locally available materials also makes it more economical and sustainable compared to proprietary UHPC products *(5)*.

## 1.2. Literature Review

### *1.2.1. Ultra-High Performance Concrete*

UHPC is a modern type of concrete exhibiting exceptional mechanical and durability properties. These properties include compressive strength greater than 17,000 psi (120 MPa) *(6)*, high ductility when fiber reinforced, and excellent resistance to frost damage, alkali-silica-reaction, and abrasion *(2,7,8)*. UHPC's properties are achieved through careful selection of its constituent materials to ensure optimized gradation and maximized packing density as well as detailed preparation methods to properly mix and cure UHPC elements *(9)*. UHPC's unique properties provide the potential to significantly improve the service life and durability of existing concrete bridge decks.

Previous UHPC research at New Mexico State University has shown that UHPC produced with local materials and supplementary cementitious materials (SCMs), such as silica fume and class F fly ash, exhibit comparable mechanical and durability properties to proprietary UHPC mixtures *(7,9,10)*. The incorporation of locally available materials can reduce materials cost up to 70% compared to proprietary UHPC *(5,11)*.

### *1.2.2. Overlays*

Concrete bridge decks play a crucial role in providing a comfortable riding surface and protecting structural elements beneath the deck from various environmental and physical

attacks. However, exposure to environmental and mechanical distress types can lead to rapid deterioration of bridge decks that requires frequent rehabilitation or, in extreme cases, replacement. Bridge deck overlays are commonly used to extend the life of concrete bridge decks. Common overlay materials include high-performance concrete (HPC), low-slump concrete (LSC), latex-modified concrete (LMC), and polymer-based concrete (PBC). However, each of these alternatives has drawbacks such as cost, service life expectancy, or availability. Figure 1 shows a cost comparison in US dollars of the overlay alternatives mentioned, proprietary UHPC, and non-proprietary UHPC overlays assuming a 25 mm thickness. It should be noted that the cost of local UHPC in Figure 1 includes only materials cost while the other alternatives also include construction costs *(1)*.

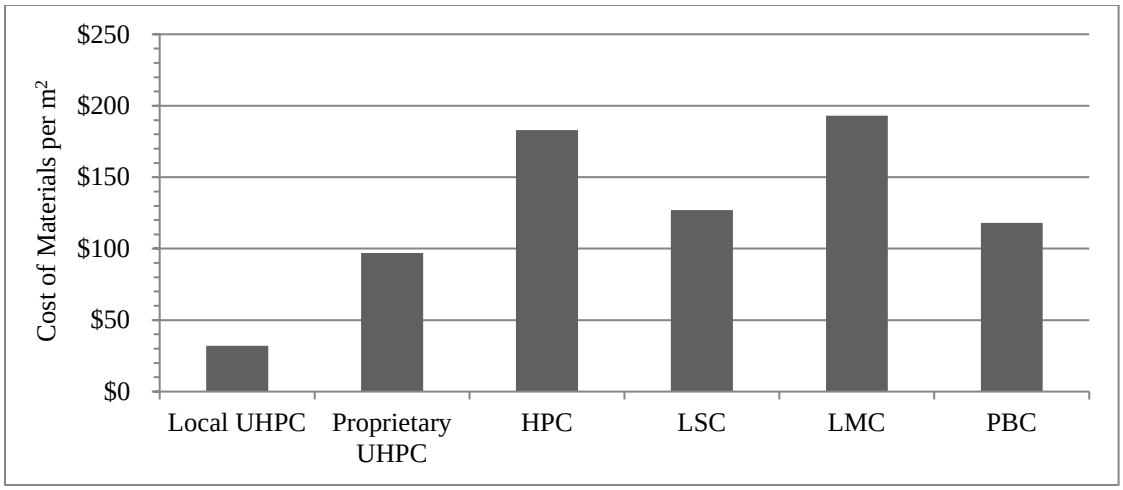


**Figure 1. Material cost per $m^2$ of different overlaying material alternatives (values taken from *(1)*).**

**Surface Preparation:** The application of concrete overlay on bridge decks prolongs the life of the deck by removing the top layer of deteriorated concrete and replacing it with an overlay material *(12)*. To prepare the surface of the deck, all deteriorated or delaminated concrete must be removed and the deck must be properly cleaned. Removal of deteriorated concrete is accomplished by scarifying. Scarifying a deck makes abrasions in the deck removing surface finishes such as paint and deck tining. It is important to note that removal of surface finishes is critical because if not adequately removed from the surface, finishes will break the bond between the substrate and the overlay. Four common mechanisms used to remove damaged concrete are presented in ICRI 310's guidelines for selecting and specifying concrete surface preparation *(12).* The four methods of scarification are impact, abrasion, pulverization, and high-pressure water erosion. These methods are briefly described as follows:

***Impact:*** This method of scarification method implements impact tools such as rotary or demolition hammers. The impact method is by far the most economically feasible and time efficient method to provide surface preparation. The drawback of using this method is the possibility of introducing micro-cracks in the system *(12).*

***Abrasion:*** Grinding stones or discs under pressure are excellent for the abrasion scarification method. Although this is a scarification method, abrasion is best for smoothing the surface rather than providing a textured surface that will contribute to bond strength of the overlay and

substrate interface *(12)*. The grinding of the surface with a rotary grinder leaves little to no surface profile.

***Pulverization:*** Steel shot-blasting and sandblasting are examples of the pulverization scarification method. The pulverization method is a good way to texture a surface that has a low risk of producing micro-cracks *(12)*. This method requires the use of compressed air mixed with an abrasive material.

***High-Pressure Water Erosion:*** Hydro-demolition is the main mechanism to achieve the high-pressure water erosion scarification method. Just like the pulverization scarification method, hydro-demolition can provide sufficient texturing of the substrate. This method also does not cause micro-cracks in the substrate material which makes it the most effective method to texturize a surface *(12)*. Hydro-demolition tools supply a water pressure against the substrate of 12,000 to 35,000 psi (83 to 241 MPa).

### *1.2.3. Factors That Influence Bond Strength*

There is a number of factors that affect the bond between the overlay material and the substrate material. According to Silfwerbrand and Beushausen the most important factors include cleanliness of the prepared surface, the presence of micro-cracks, compaction of the overlay material, and curing of concrete overlays *(13)*.

Other factors that affect the bond strength include the properties (such as workability) of the overlay material, pre-wetting of the prepared surface to promote hydration, and time (maturity) of the overlay *(14,15)*.

### *1.2.4. Stresses at the Bonded Interface*

Effectiveness of an overlay is governed by the bond between the overlay material and the substrate material *(16)*. To perform adequately, the bond between the overlay and substrate must be able to withstand the deck deformations. Deformation of the deck may be caused by: flexural deformation from loads, thermal expansion from environmental effects, and overlay shrinkage that includes chemical shrinkage and drying shrinkage.

To assess shear and tensile strengths of the bond interface, mechanical tests are typically conducted. Under laboratory conditions, it is common to perform slant-shear tests, split cylinder or split prism tests, and direct tension tests.

The slant-shear test is a widely used test to assess the bond shear strength between the substrate and overlay materials *(17)*. The slant-shear test is a test induces a combination of compression and shear stresses *(18)*. ASTM C882 / C882M is the standard slant-shear test method for assessing the shear strength of the bonded interface between two concretes *(19)*.

Two methods to assess bond tensile strength are commonly used. These two tests are the pull-off test and the split-cylinder test *(18)*. The pull-off test which consists of partially coring an overlaid specimen and applying a tensile force until failure *(18)*. The split-cylinder test is an indirect tension test that can be performed in accordance with ASTM C496 / C496M *(20)*.

To predict the response of a concrete to thermal variations caused by the environment, it is important to determine the coefficient of thermal expansion. One coefficient of thermal

expansion test that is commonly used in the south-central states is TXDOT specification Tex-428-A *(21)*. Areas subjected to large temperature changes are the areas in which the coefficient of thermal expansion is most important *(22)*. It is desirable to have thermal compatibility (similar coefficients of thermal expansion) between the overlay and substrate materials.

Concrete shrinkage can cause shear and tensile stresses at the bond interface that can, in turn, cause cracks and delamination at the bond. ACI 546 recommends using an overlay material which has the capability of shrinking without losing bond *(22)*.

## 2. OBJECTIVE

The overall objective of this study is to evaluate the potential of using UHPC produced with local materials as an overlay material on existing concrete bridge decks. To assess the potential of UHPC as an overlay material, various tests were conducted on UHPC and NSC composite specimens. Effectiveness of an overlay greatly depends on the bond strength between the overlay material and the existing concrete deck, shrinkage, and cracking properties of the overlay material. To evaluate the bond strength between the UHPC and NSC, bond tests such as slant-shear, split-cylinder, split-prism, and direct tension (pull-off) tests were performed. The specific objective of this portion of the research is to assess the ability of UHPC produced with local materials to bond adequately to substrate concrete.

Serviceability of the overlay was evaluated through the shrinkage and thermal properties of the UHPC overlay. To assess these parameters, early-age shrinkage, longer-term shrinkage, and coefficient of thermal expansion tests were conducted. The specific objective of this portion of the research is to consider thermal and shrinkage compatibility between the UHPC overlay and the substrate concrete in a manner that might illuminate insurmountable incompatibilities.

The final research task was a full-scale structural testing of a pre-stressed channel girder with a UHPC overlay. The specific objective of this task is to determine if the overlay would remain well bonded through a range of displacements that exceeded the expected in-service deformations.

## 3. SCOPE

This report presents the results of a laboratory-based research program intended to investigate the potential for using UHPC produced with local materials as an overlay material for concrete bridge decks. Methodology and results of bond strength tests that included slant-shear tests, split cylinder and split prism tests, and direct tension tests are presented.

To investigate thermal and shrinkage compatibility between the UHPC mixture and typical substrate concrete, early-age shrinkage, longer-term shrinkage, and coefficient of thermal expansion tests were conducted. Methodology and results from these tests are also presented in this report.

In the last major portion of the research program of this study, a pre-stressed channel girder was overlaid with UHPC and subjected to cyclic and ultimate loadings. The methods used for this portion of the research and the results from testing are also presented in this report.

Finally, conclusions from each of the different research aspects, along with recommendations for future research and field implementation, are provided.

# 4. METHODOLOGY

The following sections present details regarding the UHPC mixture proportions used for the overlay, bond strength tests, shrinkage and coefficient of thermal expansion tests, chloride penetration testing, slab testing, and large-scale girder testing.

## 4.1. Mixture Proportions

The UHPC mixture consisted of Type I/II Portland cement, silica fume, fly ash, high-range water reducing admixture (HRWRA), water, and 1.5% by volume of 13 mm steel fibers. The sand, cement, and fly ash were obtained from local sources while the silica fume, steel fibers, and HRWRA were acquired from regional suppliers. The NSC mixture used as the substrate material in the laboratory investigation consisted of Type I/II Portland cement, fine and coarse aggregates, water, and air-entraining admixture. Tables 1 and 2 present the mixture proportions for the concrete mixtures.

**Table 1. Mixture proportions for UHPC.**

| Material | Cement | Silica Fume | Fly Ash | Sand | HRWRA (gal/yd$^3$) | Water | Steel Fibers |
|---|---|---|---|---|---|---|---|
| **lb./yd$^3$** | 1377 | 172 | 172 | 1702 | 9.09 | 258 | 201 |

**Table 2. Mixture proportions for NSC.**

| Material | Cement | Fine Aggregate | Coarse Aggregate | Water | Air-Entraining Admixture (gal/yd$^3$) |
|---|---|---|---|---|---|
| **lb./yd$^3$** | 622 | 1263 | 1543 | 311 | 0.243 |

## 4.2. Bond Strength Tests

Three different bond strength tests were used to characterize the bond between substrate and overlay material. These tests included slant-shear, splitting tension, and direct tension tests. Each of these tests was conducted on NSC-UHPC composites with four different substrate textures

### *4.2.1. Slant-Shear*

The slant-shear tests conducted for this work followed ASTM C882 which addresses testing epoxy resin bond strength between two concrete specimen halves *(19)*. In this study, bonding agents were not used to adhere the UHPC overlay to the NSC substrate. Consequently, the bond strength, which relies on the pozzolanic nano-particles in the UHPC, was assessed.

**Slant-Shear Setup:** Specimen preparation deviated slightly from ASTM C882 in that the NSC substrate half of the slant-shear specimens were cast using a rack to support a 6 by 12 in. (152 by 305 mm) cylindrical mold at a 60 degree angle from vertical as shown in Figure 2 *(19)*. After curing the mold for 24 hours, the substrate was placed in a moist room (73°F [22.8°C] and 98% relative humidity) for 28 days to cure before being overlaid with UHPC. The slant-shear test was conducted seven days after the application of the UHPC overlay.

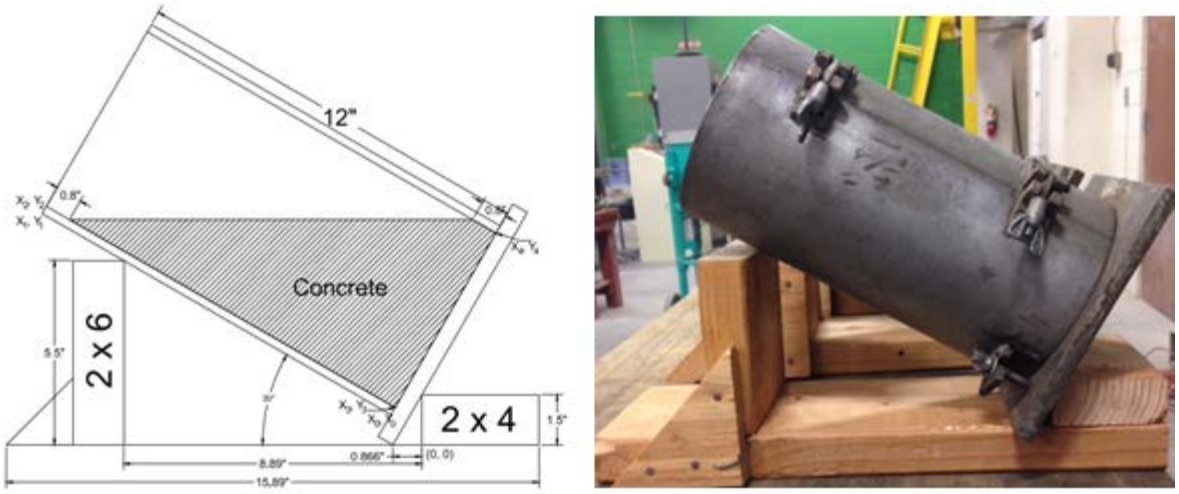


**Figure 2. Slant-shear substrate casting setup.**

**Surface Preparation:** The surface of the substrate was textured using mechanical hand-held grinders. The depths of the texture were measured in accordance to ASTM E965 *(23)*. The textures were characterized as 1) lightly ground with a depth of 0.002 in. (0.05 mm), 2) horizontal grooves with a depth of 0.035 in. (0.9 mm), 3) cross-hatched with a depth of 0.063 in. (1.6 mm), and 4) rough with a depth of 0.11 in. (2.8 mm). Photographs of surfaces with these textures are provided in Figure 3.

**Figure 3. Surface texturing on substrate specimens, 0.002 in. (0.05 mm), 0.035 in. (0.9 mm), 0.063 in. (1.6 mm), and 0.11 in. (2.8 mm), from left to right, respectively.**

**Slant-Shear Testing:** The slant-shear specimens were tested in compression, as shown in **Figure 4**, until failure. Three possible failure modes can occur that include failure in the UHPC overlay, failure of the bond, and failure in the substrate. Shear strength was calculated using Equation 1.

$$\tau_n = \frac{P}{A}\sin(\alpha)\cos(\alpha) \qquad [1]$$

where:
$\tau$ = shear stress,
P = ultimate load,
A = cross sectional area, and
$\alpha$ = angle of the bonded interface from horizontal (60°).

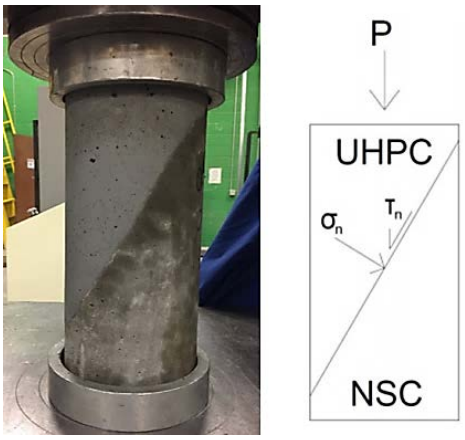


**Figure 4. Slant-shear test setup.**

### *4.2.2. Split Cylinder*

Split-cylinder tests were conducted in accordance with ASTM C496 using specimens produced in substrate and UHPC halves to test the bond strength of the UHPC-NSC composite specimen using indirect tension *(20)*.

**Split Cylinder Setup:** The NSC substrate was cast by laying the 6 by 12 in. (152 by 305 mm) cylinder mold horizontal and filling it halfway. After curing in the mold for 24 hours, the substrate was placed in a moist room (73°F [22.8°C] and 98% relative humidity) to cure for 28 days. After 28 days, the overlay was applied. After curing in the mold for 24 hours, the UHPC-NSC composite specimen was cured at ambient conditions (68°F [20°C] and 30% relative humidity) until the split-cylinder test was conducted seven days after the application of the UHPC overlay. Ambient curing conditions were used for the UHPC overlay to simulate worst-case conditions for a bridge deck overlay.

**Surface Preparation:** The NSC substrate specimens were textured in the same manner, and using the same depths (Figure 3), as the slant-shear specimens.

**Split Cylinder Test:** The procedure for the split cylinder tests followed ASTM C496 with the added condition that the bonded interface was oriented vertically (in the direction of loading) as shown in Figure 5 *(20)*. This arrangement ensured that the bonded interface of the UHPC-NSC composite specimen was loaded in indirect tension and allowed the bond strength to be calculated using Equation 2.

$$f_s = \frac{2P}{\pi dh} \qquad [2]$$

where:
$f_s$ = splitting tensile strength,
P = ultimate load,
d = specimen diameter, and
h = specimen height/length.

**Figure 5. Split cylinder test setup.**

### *4.2.3. Split Prism*

The split-prism test was conducted with modifications to ASTM C496 *(20)*. The modification was that a prismatic specimen was produced and tested instead of a cylindrical specimen. The split-prism test was implemented to assess bond strength through an indirect tension test using prismatic specimens that are easier to produce and test.

**Split Prism Setup:** The NSC substrate was cast using a 3x4x16 in. (76x102x406 mm) beam mold filled half-way with NSC. After curing in the mold for 24 hours, the NSC substrate was placed in a wet room for 28 days to cure. After 28 days, the UHPC overlay was applied and left to cure at ambient conditions for seven days. Six days after the overlay was applied, the composite beams were cut into three pieces with lengths of 4 in. (102 mm). Split-prism tests were conducted seven days after the application of the UHPC overlay.

**Surface Preparation:** The NSC substrate specimens were textured in the same manner as the split-cylinder and slant-shear specimens. The texture depths were again measured in accordance with ASTM E965, and the same textures (presented in Figure 3) were used *(23)*.

**Split Prism Test:** The split-prism test was performed in the same manner as the split-cylinder test. The bond of the composite was in line with the load as shown in Figure 6. The bond strength was calculated using a modified version of Equation 2 that is provided in Equation 3.

$$f_s = \frac{2P}{\pi l w} \qquad [3]$$

where:
$f_s$ = splitting tensile strength,
P = ultimate load,
l = specimen length, and
w = specimen width (vertical dimension of specimen during testing).

**Figure 6. Split prism test setup.**

### *4.2.4. Direct Tension*

Direct tension testing was conducted to evaluate the bond strength of the UHPC-NSC composite specimens under direct tension that could occur in bridge deck overlay if the overlay experienced curling.

**Direct Tension Setup:** As with the split-prism specimens, the NSC substrate was cast using a 3x4x16 in. (76x102x406 mm) beam mold filled half-way with NSC. After 24 hours, the NSC substrate was placed in a wet room for 28 days to cure. After 28 days, the UHPC overlay was applied and left to cure at ambient conditions for seven days. Six days after the overlay was applied, 1.875 in. (47.6 mm) specimens were cored out of the beam as shown in Figure 7. The specimen was then bonded to end plates using epoxy. The direct tension test was conducted seven days after the overlay was applied.

**Figure 7. Direct tension specimens.**

**Surface Preparation:** The NSC substrate was textured in the same manner as the slant-shear specimens using the same depths used for the previous specimens (Figure 3).

**Direct Tension Test:** Figure 8 illustrates the attachment of eye-bolts to the end plates epoxied to the specimen. The eye-bolts served as pivots at both ends of the specimen during loading so

that concentric loading was ensured. The bond strength was calculated by using the ultimate load during testing in Equation 4.

$$T = \frac{P}{A_c} \quad [4]$$

where:
T = tensile strength,
P = ultimate load, and
$A_c$ = cross-sectional area of the specimen.

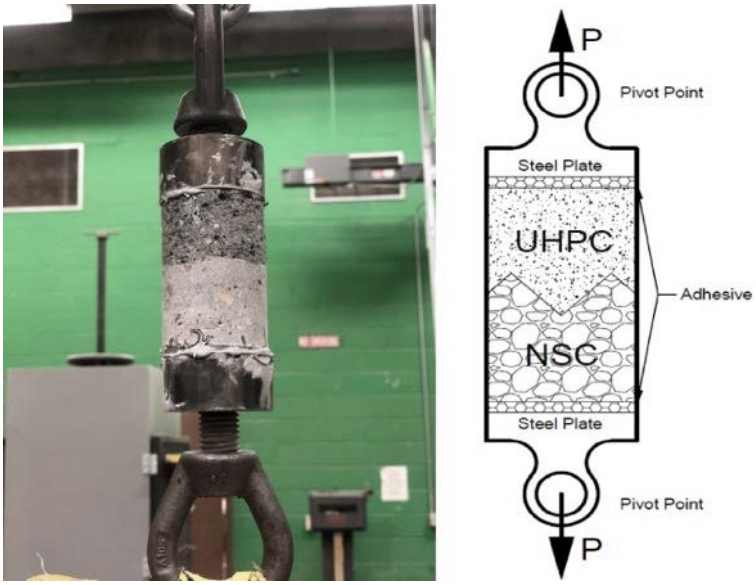


**Figure 8. Direct tension test setup.**

## 4.3. Shrinkage and Temperature Effects

### *4.3.1. Early-Age Shrinkage*

Shrinkage in the UHPC is important because it will cause shear stress on the bond between the overlay material and the mature substrate concrete. Shrinkage of the overlay material can also cause curling, which can produce direct tension on the bond between the overlay and the substrate.

**Early-Age Shrinkage Setup:** No standard test specifications are available for early age shrinkage testing, so a test method developed by Holt *(24)* was adopted. This test method was used for previous research at NMSU by *(25)* and *(10)*. The early-age shrinkage specimen was a 6x6x24 in. (152x152x610 mm) UHPC beam. The testing apparatus consisted of a steel frame that was placed over the mold for the UHPC shrinkage specimen so that it spanned the mold in the longitudinal direction. The beam mold was lined with plastic, talc powder, and another layer of plastic to minimize friction between the UHPC shrinkage specimen and the beam mold. As the UHPC shrinkage specimen was cast, steel hangers supported by the steel frame were embedded into the UHPC beam to a depth of 1 in. (25 mm) at a location that was 1 in.

(25 mm) from the ends of the beam mold. Linearly variable displacement transducers (LVDTs) that were supported by the steel frame were used to monitor movement of the hangers caused by shrinkage. A photograph of the experimental setup for the early-age shrinkage test is shown in Figure 9.

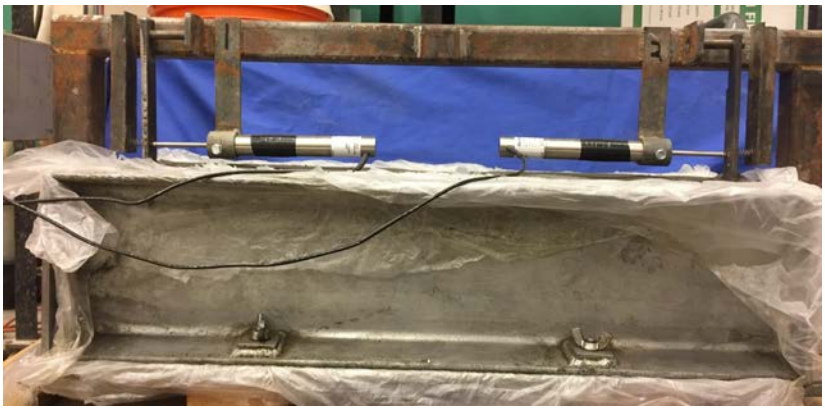

**Figure 9. Early-age shrinkage setup.**

**Early-Age Shrinkage Test:** The early-age shrinkage test ran for seven days with LVDT readings collected every 15 seconds. The gage length of the specimen was 22 in. (559 mm), from hanger to hanger. The change in length of the specimen was computed using the measurements of the two LVDTs shown in **Figure 9.** Change in length obtained from the LVDT measurements was used in Equation 5 to calculate the shrinkage strains in the UHPC.

$$\varepsilon = \frac{\Delta L}{L} \qquad [5]$$

where:
ε = strain,
ΔL = change in length, and
L = gage length.

### *4.3.2. Longer-Term Shrinkage*

Longer-term shrinkage in overlay concrete also contributes to shear stresses and direct tension on the bonded interface. Therefore, longer-term shrinkage of UHPC was also characterized.

**Longer-Term Shrinkage Setup:** Longer-term shrinkage was measured according to ASTM C157 *(26)*. The longer-term shrinkage specimens were 3x4x16 in. (76x102x406 mm) prisms with gage studs (contact points) cast into the ends of the specimens. After curing in the mold for 24 hours, the longer-term UHPC shrinkage specimens were cured in a wet room for seven days. After the seven-day wet cure, the specimens were placed in ambient conditions for the remainder of the shrinkage monitoring.

**Longer-Term Shrinkage Test:** Shrinkage monitoring began right after the beams were removed from the molds. Changes in length were measured using a comparator as shown in Figure 10. Measurements were recorded every day for 28 days that included the seven days of wet curing and the remaining time at ambient conditions.

**Figure 10. Longer-term shrinkage test setup.**

Shrinkage strains for the longer-term shrinkage tests were computed using the changes in length from the comparator readings and Equation 5.

### *4.3.3. Coefficient of Thermal Expansion*

Coefficient of thermal expansion tests were conducted on 3x4x16 in. (76x102x406 mm) UHPC prism specimens that were wet cured for 28 days prior to testing. The test was conducted following the procedure in Tex-428-A *(21)*. In this method, specimens are allowed to reach equilibrium in a water bath at 50°F (10°C). The temperature is then raised to 122°F (50°C). Finally, the temperature is lowered to 50°F (10°C) again. Length changes of the specimen being tested are monitored during these temperature swings.

## 4.4. Rapid Chloride Permeability Tests

Rapid chloride permeability tests (RCPTs) were conducted to assess the corrosion susceptibility of fibers in the UHPC. The RCPTs were conducted according to ASTM C1202 *(27)*. For each test, a 2 in. (51 mm) slice was cut from a 4 by 8 in. (102 by 203 mm) cylindrical specimen. The slices were vacuumed for three hours in a desiccator before being submerged in deionized water for 18 hours. UHPC slices were then placed in the testing cell shown in Figure 11. A power supply maintained a 60V DC voltage across the cell with the negative lead attached to the NaCl reservoir and the positive lead attached to the NaOH reservoir. A multi-meter was used to measure the current passing through the specimen at 30-minute intervals over a six-hour period. RCPTs were performed on two specimens, one fiber reinforced and one that was not fiber reinforced.

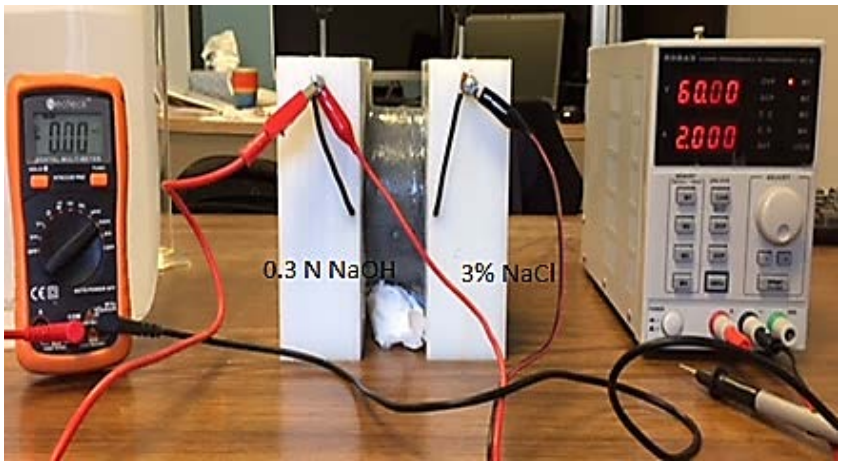


**Figure 11. RCPT setup.**

## 4.5. Slab Tests

To investigate the combined effects of temperature and shrinkage on slabs with UHPC overlays, the behaviors of five NSC reinforced slabs with dimensions of 3x3 ft. (0.9x0.9 m) with varied thickness were monitored. Each slab had a reinforcement mesh consisting of six bars, three in each direction. The slab design and instrumentation layout is illustrated in **Figure 12**. Additionally, the specimens had varied parameters that included exposure condition, thickness of NSC slab, reinforcement bar size, and application of overlay. The specific characteristics for each slab are provided in Table 3, and were selected such that at least two slabs can be compared with just a single parameter variation per pair of slabs.

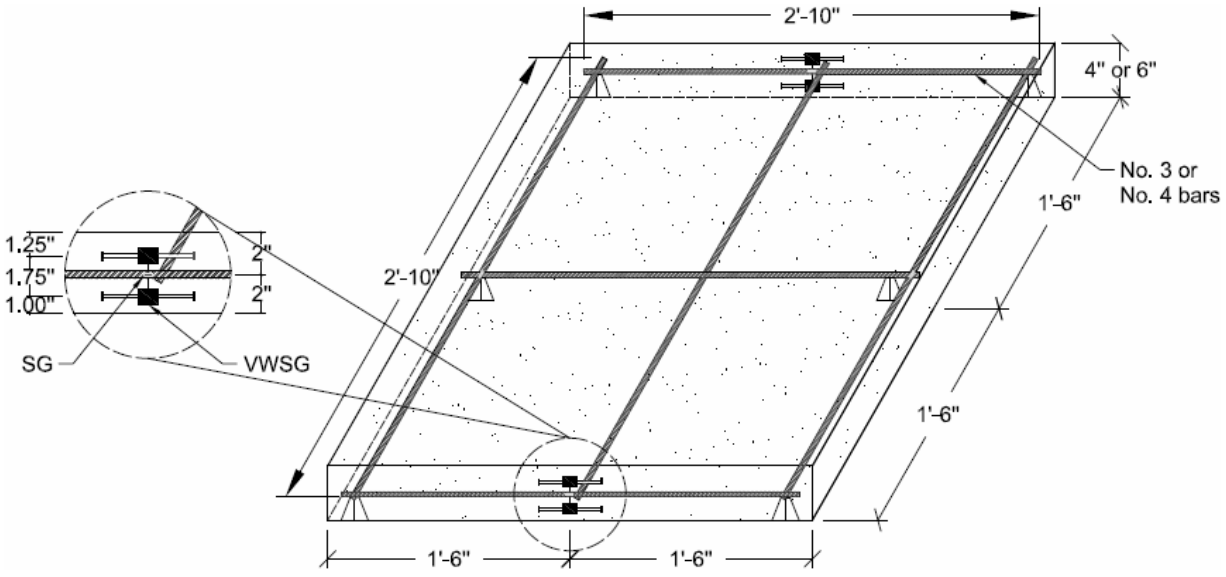


**Figure 12. Slab design.**

**Table 3. Specimens' characteristics.**

| Specimen | Exposure Condition | Thickness NSC in. (cm) | Bar Size | Overlay | Thickness UHPC in. (cm) |
|---|---|---|---|---|---|
| **Slab 1** | Controlled | 4 (10.16) | No. 3 | Yes | 1 (2.54) |
| **Slab 2** | Controlled | 4 (10.16) | No. 3 | No | – |
| **Slab 3** | Environmental | 4 (10.16) | No. 4 | Yes | 1 (2.54) |
| **Slab 4** | Environmental | 6 (15.24) | No. 4 | Yes | 1 (2.54) |
| **Slab 5** | Environmental | 4 (10.16) | No. 3 | Yes | 1 (2.54) |

All slabs used the same NSC mixture proportions, provided by a local ready-mix company. The air-entrained mixture proportions are provided in Table 4, which include a 1-in (25.4 mm) aggregate top size, and had a design strength of 4500 psi (31.0 MPa). Furthermore, the water-to-cement ratio used in this mix was 0.39, with a slump of 4 +/- 1 in. (102 +/- 25 mm), and a unit weight of 143.0 lb./ft.$^3$ (2290 kg/m$^3$).

**Table 4. Mixture proportions of NSC.**

| Material Type | Specific Gravity | Quantity lb/yd$^3$ (kg/m$^3$) |
|---|---|---|
| Cement | 3.15 | 508 (230) |
| Fly Ash | 2.35 | 127 (57.6) |
| Fine Aggregate | 2.6 | 1225 (556) |
| Coarse Aggregate | 2.55 | 1750 (794) |
| Water | 1 | 250 (113) |
| | **Total** | 3860 (1751) |

Two types of sensors were used in this research, strain gauges (SGs) with a length of 0.08 in. (2 mm) attached to the steel reinforcement, and vibrating wire strain gauges (VWSGs) with a length of 6.75 in. (171.4 mm) embedded in the NSC substrate. To determine changes in strain, the VWSG frequency is measured by sensors connected to a datalogger. The change in frequency was recorded at 10-minute intervals, which was the average of the change in frequency measured every two minutes within the 10-minute period. The average change in frequency was used to determine the strain in the substrate.

## 4.6. Preparation of NSC Slabs

Preparation of the slabs started with the placement of the sensors. The SGs were placed at the midpoint of the length of the steel bars located near the edges of the slabs. The VWSGs were placed above and below the rebar at mid-span of the slab as shown in Figure 12. After the SGs were placed on the reinforcement, the meshes were placed in the formwork. The VWSGs were then tied with steel wire from the middle of the sensors to the reinforcement, leaving approximately 1.75 in. (43.8 mm) between gauges. Photographs of the sensors and of the reinforcement mesh after placement in the formwork are shown in Figure 13.

**Figure 13. Sensors, including (a) vibrating wire strain gauges, (b) strain gauges, and (c) location of sensors before placement of NSC.**

The five slabs were cast at the same time. The NSC was dispensed one slab at a time, and a vibrator was used to ensure good consolidation. When the desired thickness was met, the surface of each slab was floated. Once casting was complete, the slabs were trowel finished and covered with plastic. After 24 hours, the slabs were wetted twice a day for three days. Six days after casting NSC slabs, the formwork was removed. Some images of the slab construction are shown in Figure 14.

**Figure 14. Slab construction: (a) formwork and sensors and (b) placement of NSC substrate.**

## 4.7. Preparation of UHPC Overlay Deck

The surface preparation of the NSC slabs was conducted at an age of 30 days. The surface was prepared by using air hammers and chisels to chip away the surface concrete and minimal hand grinding around the edges until the aggregates were exposed. Texture depth was measured following ASTM E965 in each quadrant of each slab using a 0.845 fl. oz. (25 ml) volume of glass spheres *(23)*. The average depths obtained using this procedure are provided in Table 5.

**Table 5. Results of macro-texture depth using volumetric technique.**

| **Specimen** | **Depth I** in. (mm) | **Depth II** in. (mm) | **Depth III** in. (mm) | **Depth IV** in. (mm) |
|---|---|---|---|---|
| **Slab 1** | 0.089 (2.28) | 0.064 (1.63) | 0.096 (2.44) | 0.107 (2.73) |
| **Slab 2** | 0.086 (2.19) | 0.069 (1.75) | 0.086 (2.19) | 0.086 (2.19) |
| **Slab 3** | 0.072 (1.83) | 0.054 (1.37) | 0.060 (1.53) | 0.061 (1.56) |
| **Slab 4** | 0.117 (2.99) | 0.153 (3.89) | 0.125 (3.18) | 0.102 (2.58) |
| **Slab 5** | 0.111 (2.81) | 0.089 (2.25) | 0.072 (1.83) | 0.080 (2.02) |

After the substrate was textured, plywood was used as formwork for the application of the UHPC overlay. The surface was saturated for 24 hours prior to the placement of UHPC. Once the surface and the formwork were ready, the UHPC overlay was placed. The UHPC for each overlay was mixed next to the slab (one batch per slab overlay). Once the UHPC mixture was ready, and workable enough to be applied, the UHPC was cast on the NSC slabs. The surface was then finished and covered with plastic. Figure 15 shows some of the steps during the placement of the UHPC overlay. Twelve hours after placing each UHPC overlay, wet burlap was placed on top of the UHPC. The burlap was re-wetted every 12 hours for seven days.


**Figure 15. Preparation of UHPC overlay: (a) saturated rough surface with exposed aggregates before UHPC application, (b) workable consistency of UHPC mixture, and (c) tools used during the surface finishing of the overlay.**

## 4.8. Test Specimens

To verify the properties of the materials used in this research, tests were performed on companion specimens of each batch that was used in the project. Compressive strengths were obtained at 28 days from 6 by 12 in. (152 by 305 mm) cylindrical specimens of NSC by testing according to ASTM C39/C 39M *(28)*. UHPC compressive strengths were obtained by testing 3.94 in. (100 mm) cubes according to BS 1881 *(29)*. Flexural strength tests were performed at 28 days on 3x4x16 in. (76x102x406 mm) prisms for NSC following ASTM C78/C78M [30]. Similar 3x4x16 in. (76x102x406 mm) prisms containing UHPC were tested according to ASTM C1609/C1609M at 28 days of age *(31)*. The modulus of rupture (first cracking) was estimated as:

$$R = \frac{PL}{bd^2} \qquad [6]$$

where:
R = modulus of rupture,
P = maximum applied load indicated by the testing machine,
L = span length,
b = average width of specimen at fracture, and
d = average depth of specimen at fracture.

Static modulus of elasticity tests were performed on 6 by 12 in. (152 by 305 mm) cylindrical specimens for NSC and UHPC at 28 days of age following ASTM C469/C469M *(32)*. The modulus of elasticity was computed as:

$$E = \frac{(S_2 - S_1)}{(\varepsilon_2 - 0.000050)} \quad [7]$$

where:
E = modulus of elasticity,
$S_2$ =stress corresponding to 40% of ultimate load,
$S_1$= stress corresponding to a longitudinal strain, $\varepsilon_1$, of 50 millionths, and
$\varepsilon_2$= longitudinal strain produced by stress $S_2$.

## 4.9. Channel Girder Tests

### *4.9.1. Girder Design*

The design for girder H-PS-C-300-R-UO (see naming convention provided in Figure 16) was prepared in accordance with AASHTO load and resistance factor design (LRFD) bridge design specifications *(32)*. The compressive strength ($f'_c$) met standard NMDOT mixture proportion requirements for pre-stressed high-performance concrete (HPC) bridge girders, and a design release strength of $0.75f'_c$ was used. The design values are summarized in Table 6.

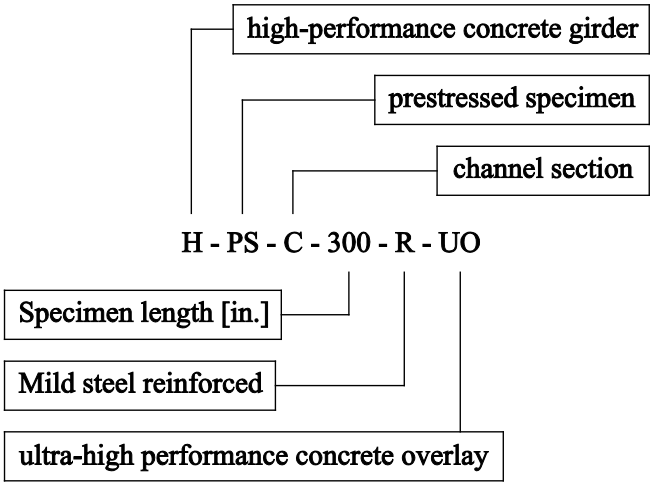


**Figure 16. Naming convention for girder H-PS-C-300-UO.**

**Table 6. H-PS-C-300-R-UO girder design parameters.**

| | |
|---|---|
| **Compressive Strength at Release, $f'_{ci}$ (ksi)** | **7.0** |
| **Compressive Strength at Design, $f'_c$ (ksi)** | 9.5 |
| **Section Depth, d (in.)** | 15.0 |
| **Girder Width, $b_f$ (in.)** | 48.0 |
| **Flange Depth, $d_f$ (in.)** | 4.0 |
| **Stem Width, $b_w$ (in.)** | 7.0 |
| **Cross-sectional Area, $A_c$ ($in^2$)** | 346 |
| **Strand Ultimate Strength, $f_{pu}$ (ksi)** | 270 |
| **Mild Steel Yield Strength, $f_{sy}$ (ksi)** | 60.0 |
| **1 ksi = 6.895 MPa, 1 in. = 25.4 mm, 1 $in^2$ = 645.16 $mm^2$** | |

As seen in Figures 17 and 18, the design section was pre-stressed with six 270-ksi (1,860-MPa), 0.60-in. (15-mm) diameter, low-relaxation, fully-bonded pre-stressing strands per stem. Each strand was pre-tensioned to 202.5 ksi (1,396 MPa), requiring the centroid of the strands to be at 6.0 in. (152 mm) from the extreme compression fiber to adequately resist a total jacking force of approximately 527 kips (2,345 kN). Shear reinforcement was provided in each stem in the form of No. 3 (No. 10) stirrups, which were placed in pairs. After bursting reinforcement requirements were satisfied, shear reinforcement was placed at a 6-in. (152-mm) on-center in the high-shear regions [24 in. (610 mm) from each end], and then the spacing was increased to 8 in. (203 mm) over the remaining length of the girder. The outer bar of the hoop was bent to accommodate shear keys (not present on the test specimens to facilitate instrumentation during testing). Transverse No. 5 (No. 16) bars were spaced at 6-in. (152-mm) increments along the full length of the beam in the flange and extended into the stems. Alternating No. 3 (No. 10) and No. 4 (No. 13) bars provided longitudinal reinforcement in the deck (Figure 15). Steel bearing plates [9 in. (230 mm)] were embedded in the stems at each end of the beam at bearing locations.

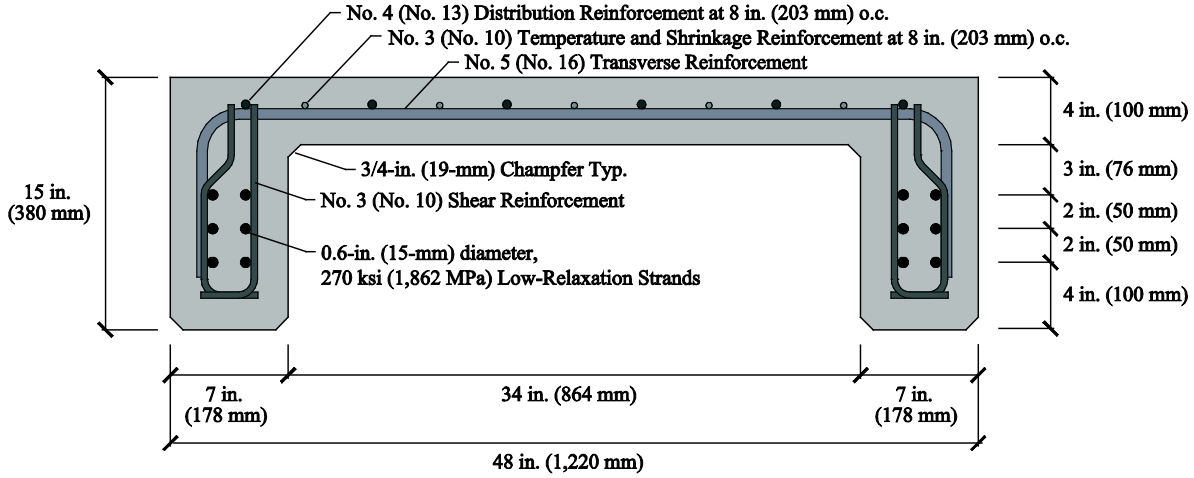


**Figure 17. Reinforcement layout for girder H-PS-C-300-R-UO cross-section.**


**Figure 18. Girder H-PS-C-300-R-UO (a) reinforcement before casting and (b) after pre-stress transfer.**

### *4.9.2. UHPC Overlay*

Preparations for placement of a UHPC overlay on the surface of girder H-PS-C-300-R-UO were conducted at the Structural Systems and Materials Testing Laboratory (SSMTL) at New Mexico State University (NMSU). The girder surface was first textured to ensure adequate bond between the overlay and girder concrete (Figure 19a). This was accomplished by chipping away the top layer of finished girder surface using handheld compressed air hammers. The surface was thoroughly cleaned and the texture depth was determined according to ASTM E965 (2015) *(23)* by application and measurement of eight 3.38 fl. oz. (100 mL) samples of glass microbeads at evenly spaced locations along the 25 ft. (7.62 m) length of the girder as shown in Figure 19. The results of this procedure, provided in Table 7, yielded a mean texture depth for the girder surface of 0.097 in. (2.47 mm). Research has shown when UHPC is used as overlay material on a saturated subsurface, depths between 0.025 in. (0.64 mm) and 0.051 in. (1.29 mm) are adequate for achieving satisfactory bond strength *(34)*.

(a) (b)

**Figure 19. (a) Textured girder substrate and (b) determination of texture depth.**

**Table 7. Mean texture depth (MTD).**

| Test No. | Avg. Diameter in. (mm) | MTD in. (mm) |
|---|---|---|
| **1** | 9.50 (241) | 0.086 (2.19) |
| **2** | 8.06 (205) | 0.120 (3.04) |
| **3** | 8.69 (221) | 0.103 (2.61) |
| **4** | 8.69 (221) | 0.103 (2.61) |
| **5** | 9.44 (240) | 0.87 (2.22) |
| **6** | 9.06 (230) | 0.095 (2.40) |
| **7** | 9.75 (248) | 0.082 (2.08) |
| **8** | 8.75 (222) | 0.101 (2.58) |
| **Average** | | 0.097 (2.47) |

Following construction of formwork, the textured surface of girder H-PS-C-300-R-UO was covered in soaked burlap and plastic to adequately hydrate the surface for approximately 36 hours prior to placement of the UHPC. Mixing was conducted using a 4.25 $ft^3$ (0.120 $m^3$) portable vertical shaft mixer, but due to the density of the UHPC mixture, batch sizes were limited to approximately 1.25 $ft^3$ (0.035 $m^3$). Seven batches and accompanying samples were required to provide the 100 $ft^2$ (9.30 $m^2$) girder surface with a nominal 1.0 in. (25 mm) thick

overlay. Each batch was mixed and placed consecutively, and the concrete covered with plastic to reduce moisture loss and surface cracking. Care was taken to keep the concrete near the end of each pour agitated until placement of the next batch to ensure proper consolidation and avoid development of cold joints. Various samples were cast with each batch for determination of mechanical properties.

Approximately 24 hours after placement, adequate time for initial set, the overlay was covered with soaked burlap and plastic for six days to promote hydration of the UHPC. Figure 20 provides photos of the casting process and the finished overlay surface.


**Figure 20. UHPC overlay on girder H-PS-C-300-R-UO (a) during placement and (b) prior to testing.**

## 4.10. Measured Material Properties

Several material properties were investigated in this study that are related to the design and testing of girder H-PS-C-300-R-UO. Testing included the use of applicable ASTM International Standards, as well as additional relevant international procedures when necessary to determine the stress-strain behaviors of the materials used for design purposes. The material properties investigated are described in the following sections.

### *4.10.1. Concrete Compressive Strength*

Compressive strengths were determined for girder H-PS-C-300-R-UO and for all UHPC overlay concrete batches. For the HPC, cylinder specimens with nominal diameters and lengths of 4.0 in. (102 mm) by 8.0 in. (203 mm), respectively, were tested according to ASTM C39 *(28)*. For UHPC, 3.94 in. (100 mm) cubes were tested according to British Standard (BS) 1881 Part 116 *(29)*. Cube specimens were selected for compressive strength testing of UHPC to eliminate the need for end preparation and grinding that cylindrical specimens would require.

Specimens were tested using a 1,000-kip (4,450-kN) capacity compression machine. The specimens were placed between high-yield steel auxiliary platens to evenly distribute load, lightly oiled to reduce lateral confinement. HPC specimens were tested at a rate of 2,100 psi/min (14.5 MPa/min). Due to the higher compressive strengths exhibited by UHPC, an increased load rate of 9,000 psi/min (62.0 MPa/min) was used for all UHPC compression specimens. Compressive strengths are summarized for HPC cylinder specimens and UHPC cube specimens in Table 8 and Table 9, respectively.

**Table 8. Compressive strengths of HPC 4.0 in. (100 mm) cylinder specimens - girder H-PS-C-300-R-UO.**

| Specimen No. | Age (days) | Compressive Strength ksi (MPa) |
|---|---|---|
| **1** | 1 | 8.38 (57.8) |
| **2** | 1 | 8.28 (57.1) |
| **Average** | | 8.33 (57.4) |
| **3** | 28 | 12.00 (82.8) |
| **4** | 28 | 11.35 (78.2) |
| **Average** | | 11.68 (80.5) |
| **5*** | 1248 | 11.75 (81.0) |
| **6*** | 1248 | 11.54 (79.6) |
| **Average** | | 11.65 (80.3) |

*Sample tested on day of failure test, April 26, 2018

**Table 9. Compressive strengths of UHPC 3.94 in. (100 mm) cube specimens - girder H-PS-C-300-R-UO.**

| Specimen No. | Age (days) | Compressive Strength ksi (MPa) |
|---|---|---|
| **1** | 28 | 16.49 (113.7) |
| **2** | 28 | 16.98 (117.1) |
| **3** | 28 | 15.50 (106.8) |
| **4** | 28 | 16.26 (112.1) |
| **5** | 28 | 15.69 (108.2) |
| **6** | 28 | 15.66 (107.9) |
| **7** | 28 | 16.76 (115.6) |
| **8** | 28 | 17.49 (120.6) |
| **9** | 28 | 14.58 (100.5) |
| **10** | 28 | 16.24 (112.0) |
| **Average** | | 16.16 (111.5) |
| **11*** | 34 | 18.08 (124.7) |
| **12*** | 34 | 17.51 (120.7) |
| **Average** | | 17.80 (112.7) |

***Samples tested on day of failure test, April 26, 2018

### *4.10.2. UHPC Modulus of Elasticity*

Modulus of elasticity for the UHPC overlay of girder H-PS-C-300-R-UO was determined according to ASTM C469 *(32)*. Testing was conducted on two cylindrical specimens cast during placement of the girder overlay with nominal diameter and length dimensions of 6.0 in. (152 mm) by 12.0 in. (305 mm), respectively. Specimens were tested using a 1,000-kip (4,450-kN) capacity compression machine. The specimens were mounted with a compressometer that was instrumented to measure vertical displacement during a test. The results, presented in Table 10 below, yielded an average modulus of elasticity of $5.73 \times 10^6$ psi (39.5 GPa).

**Table 10. UHPC modulus of elasticity - girder H-PS-C-300-R-UO.**

| Specimen No. | Age (days) | Modulus of Elasticity psi (GPa) |
|---|---|---|
| **1** | 38 | $5.88 \times 10^6$ (40.5) |
| **2** | 38 | $5.58 \times 10^6$ (38.5) |
| **Average** | | $5.73 \times 10^6$ (39.5) |

### *4.10.3. Mild Steel Reinforcement*

Girder H-PS-C-300-R-UO was provided mild steel reinforcement as specified by AASHTO LRFD Bridge Design Specifications *(33)*, and all reinforcement met ASTM A615 requirements *(35)*. To determine the stress-strain behavior of the mild steel reinforcement, four 8.0 in. (203 mm) representative samples of No. 3 (No. 10), No. 4 (No. 13), and No 5 (No. 16) bars were tested for each bar size. The samples were taken from the same stock as the bars used for reinforcement of girder H-PS-C-300-R-UO. By determining these stress-strain relationships, strain-compatibility analyses may be used to predict behavior that can be compared to the actual mechanical behavior of the full-scale specimens exhibited during flexural testing.

Mild steel reinforcement samples were tested according to ASTM A370 *(36)* using a 20.0-kip (89.0-kN) capacity universal testing machine and a deflection-controlled load rate of 0.02 in./min (5.1 mm/min). An extensometer was attached to the samples with a 2.0 in. (50 mm) gauge length.

The yield strength was determined as the lower yield point of the stress-strain relationship. Yield strain is determined by dividing the yield strength by the measured modulus of elasticity (Young's modulus) which is calculated as the slope of the linear-elastic portion of the stress-strain relationship. Ultimate strain is assumed to occur at a stress of 85% of maximum. These values are summarized for all reinforcing steel samples in Table 11. All samples displayed typical behavior of Grade 60 steel, as seen in Figures 21 - 23. Markers are provided indicating the points of yielding, ultimate stress, and rupture of each sample.

### *4.10.4. Pre-stressing Strands*

The pre-stressing strands used for girder H-PS-C-300-R-UO were 0.6-in. (15.2-mm) diameter Grade 270, low-relaxation strands. The high capacity of these strands exceeded the testing capabilities of available equipment at NMSU, so the strand manufacturer's tensile strength specifications were provided by the pre-caster for the batch of strands used for girder H-PS-C-300-R-UO. Yield strength of the strands was assumed to fit the AASHTO equation for yield strength ($f_{py}$) of low-relaxation strands, specified as a function of ultimate tensile strength ($f_{pu}$), presented in Equation 8 *(33)*:

$$f_{py} = 0.9 f_{pu} \qquad [8]$$

**Table 11. Summary of mild steel reinforcement stress-strain behavior - girder H-PS-C-300-R-UO.**

| Specimen | Size | Yield Stress ksi (MPa) | Yield Strain | Ultimate Stress ksi (MPa) | Ultimate Strain | Rupture Stress ksi (MPa) | Rupture Strain |
|---|---|---|---|---|---|---|---|
| **1** | No. 3 (No. 10) | 65.3 (450) | 0.0024 | 104 (716) | 0.1312 | 83.8 (578) | 0.2370 |
| **2** | No. 3 (No. 10) | 65.1 (449) | 0.0027 | 103 (713) | 0.1328 | 84.3 (581) | 0.2449 |
| **3** | No. 3 (No. 10) | 65.6 (452) | 0.0021 | 104 (717) | 0.1168 | 83.5 (576) | 0.2388 |
| **4** | No. 3 (No. 10) | 65.0 (448) | 0.0021 | 103 (712) | 0.1180 | 86.2 (595) | 0.2305 |
| **1** | No. 4 (No. 13) | 75.4 (520) | 0.0032 | 98.6 (680) | 0.1333 | 79.3 (546) | 0.2352 |
| **2** | No. 4 (No. 13) | 74.7 (515) | 0.0031 | 97.7 (673) | 0.1470 | 79.1 (546) | 0.2526 |
| **3** | No. 4 (No. 13) | 73.2 (505) | 0.0033 | 102 (701) | 0.1376 | 82.7 (570) | 0.2517 |
| **4** | No. 4 (No. 13) | 72.8 (502) | 0.0030 | 102 (700) | 0.1428 | 82.5 (569) | 0.2685 |
| **1** | No. 5 (No. 16) | 67.5 (465) | 0.0037 | 94.8 (654) | 0.1334 | 76.7 (529) | 0.2504 |
| **2** | No. 5 (No. 16) | 63.8 (440) | 0.0040 | 92.6 (639) | 0.1425 | 77.4 (534) | 0.2901 |
| **3** | No. 5 (No. 16) | 66.0 (455) | 0.0032 | 92.6 (639) | 0.1197 | 74.5 (514) | 0.2377 |

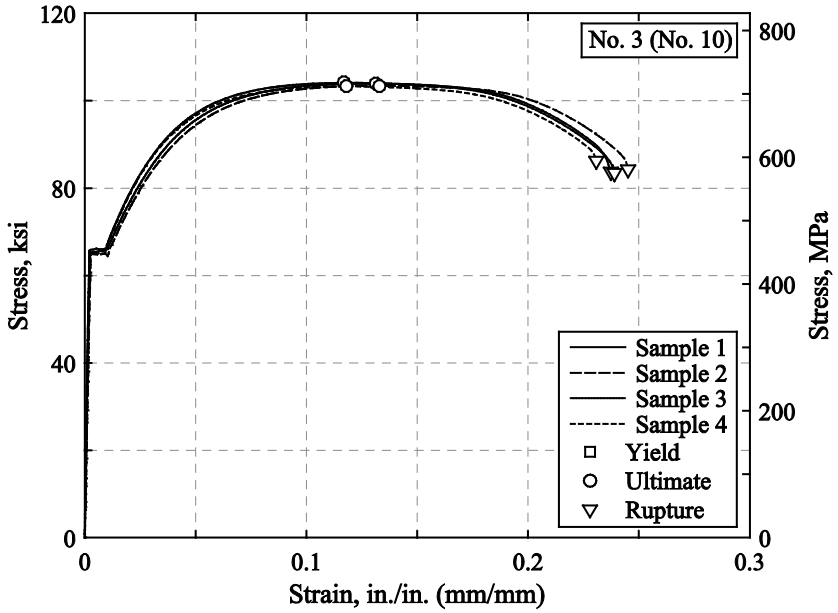


**Figure 21. Stress versus strain behavior for No. 3 (No. 10) reinforcing bar.**

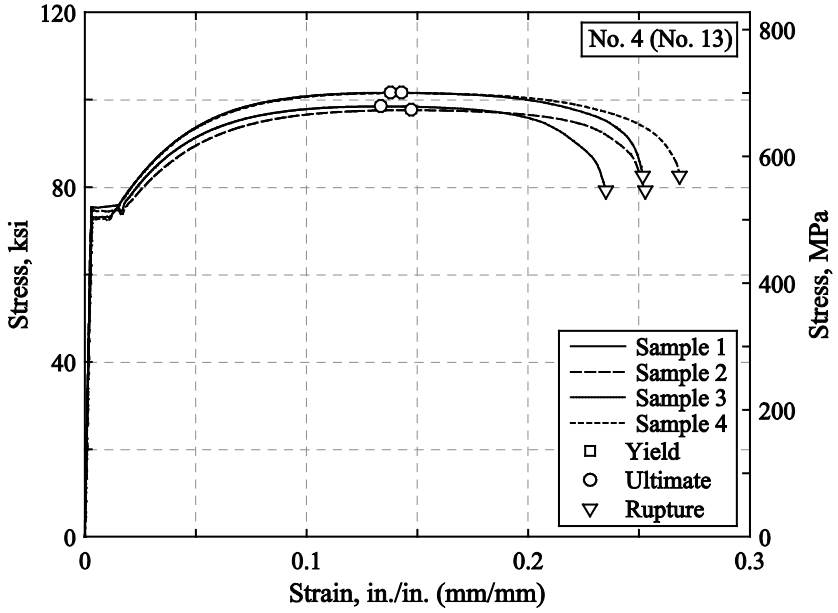


**Figure 22. Stress versus strain behavior for No. 4 (No. 13) reinforcing bar.**

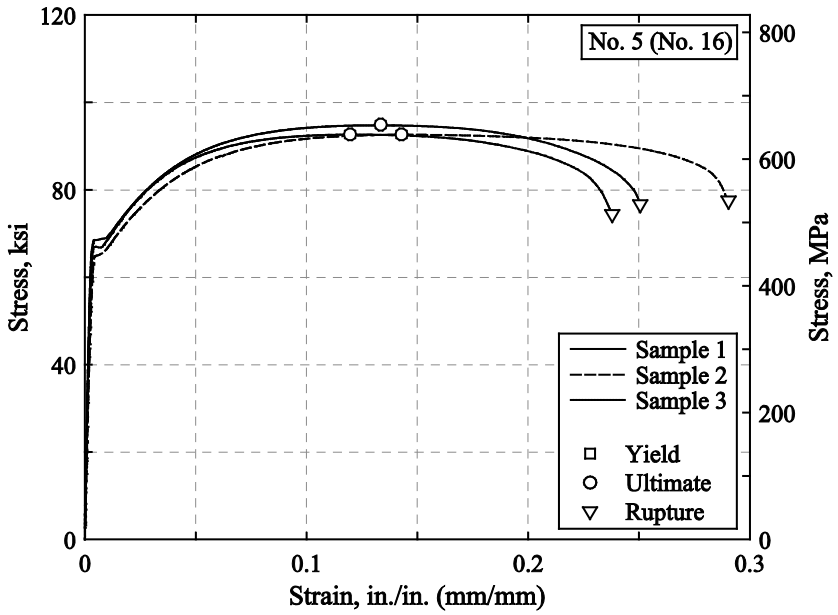


**Figure 23. Stress versus strain behavior for No. 5 (No. 16) reinforcing bar.**

Strand tensile behavior is presented in Figure 24. Markers are provided to indicate points of yielding and failure. The modulus of elasticity of strands used for this research was specified by the manufacturer to be 28,800 ksi (198.6 GPa).

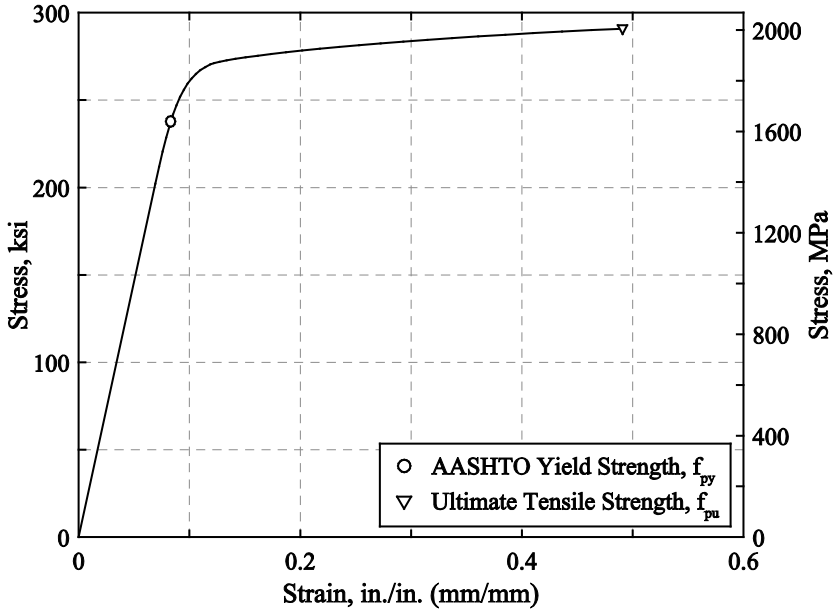


**Figure 24. Stress-strain behavior of 0.6 in. (15.2 mm) diameter grade 270 low-relaxation pre-stressing strands.**

## 4.11. Flexural Testing

Longitudinal four-point flexural testing of girder H-PS-C-300-R-UO was conducted in the SSMTL at NMSU on three separate occasions. Cyclic loading was conducted before and after the addition of the UHPC overlay, and then a final test to failure was performed. The testing setup and instrumentation are detailed in the following sections.

### *4.11.1. Test Setup and Instrumentation*

Girder H-PS-C-300-R-UO was placed on four short reinforced concrete columns and positioned beneath two, 110-kip (490-kN) capacity hydraulic actuators as shown in Figure 25. Each column was provided a steel column cap and a 4 in. (100 mm) cylindrical steel roller support. The roller supports under one end of the girder remained free to displace laterally, reducing development of axial forces.

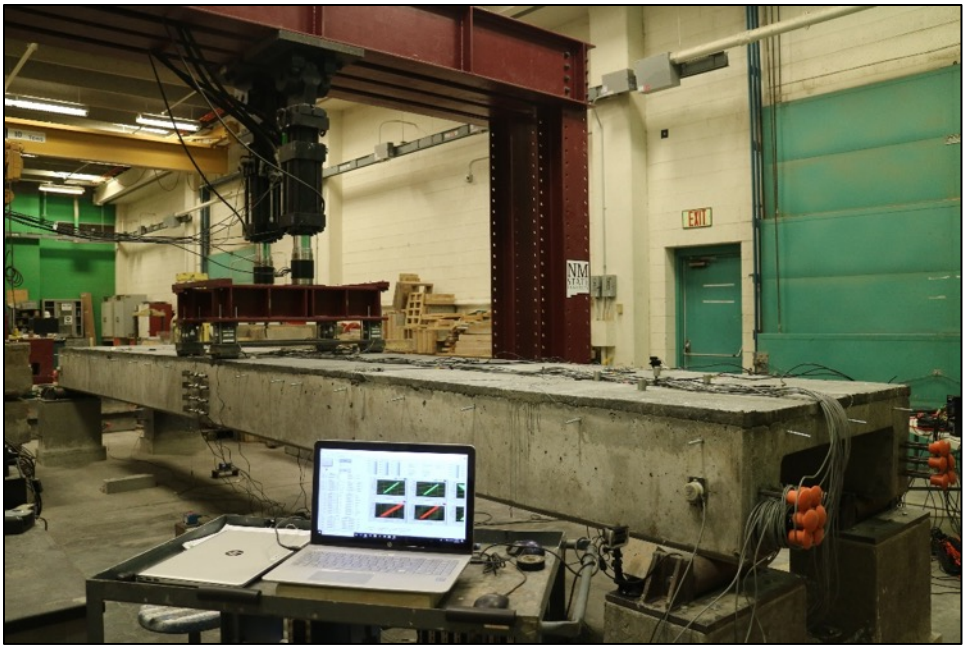

**(a)**

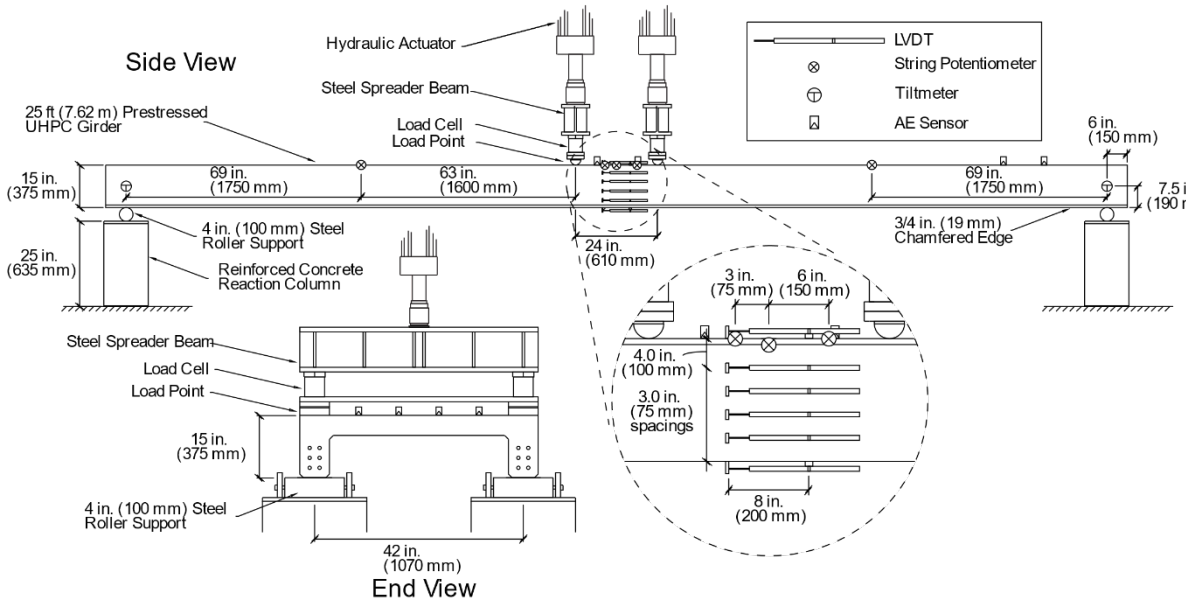


**(b)**

**Figure 25. Girder H-PS-C-300-R-UO (a) flexural testing setup and (b) instrumentation plan.**

The actuators were placed 24 in. (610 mm) apart, each 12 in. (305 mm) from mid-span, effectively creating a pure moment region. Load was applied using computer-controlled actuator displacements at set cyclic or monotonic rates and recorded by internal load cells within the actuator heads (loading rates are detailed in the following sections). As shown in Figure 25, load was distributed through steel spreader beams to 3 in. (75 mm) diameter semi-circular load points centered over each stem to create a longitudinal four-point loading scenario. The load at each point was recorded with additional load cells to capture distribution of loading.

The girder was instrumented with a range of sensors to capture the behavioral response to flexural loading (Figure 25). Electronic clinometers, also known as tiltmeters, were positioned at mid-depth of the girder over each support to record beam rotation and provide a representation of the symmetry of load application. String potentiometers were placed along the longitudinal length of the span on either side of the girder to measure deflection. Placement locations included quarter points, mid-span, and offset mid-span to avoid loss of data should the primary instrument be lost due to cracking at the application point. After the addition of the UHPC overlay, string potentiometers were offset to either side of mid-span and attached to the top surface of the overlay. Two LVDTs were applied at mid-span to the vertical face of each stem, positioned above and below the uncracked-transformed neutral axis, measuring induced compression and tension through the depth of the girder, as well as directly above and below each stem to record extreme strains. Acoustic emissions (AE) sensors were placed in regions where high shear and moment were expected near the girder end and mid-span. Strain gauges were also present, having been applied to longitudinal, transverse, and shear mild steel reinforcement prior to casting of the girder. All sensors were connected to a data acquisition system, facilitating real-time monitoring and data collection throughout testing.

### *4.11.2. Acoustic Emissions*

AE data for this research was collected using the Micro-II Digital Acoustic Emission System and a total of eight sensors attached to the girder deck or overlay surface. The sensors were placed in two groups of four in regions of expected high shear and moment near the girder end and longitudinal mid-span as shown in Figure 26a and b. The AE sensors were placed in a staggered pattern at each location to facilitate triangulation of signal detection. Data was collected throughout cyclic and ultimate loading of girder H-PS-C-300-R-UO. However, a high output of acoustic emission hits caused by the fiber reinforcement present in the UHPC overlay, contact due to load points and supports, and cracking in the HPC girder, delamination of the overlay was not discernable in the AE data.

### *4.11.3. Cyclic Loading*

Prior to casting the UHPC overlay, flexural testing of girder H-PS-C-300-R-UO began with a cyclic loading sequence, herein referred to as Cyclic Loading 1 (CL1). Using the load configuration shown in Figure 25, the girder was first loaded at a constant rate 0.1 in./min (2.54 mm/min) to the desired mid-span deflection discussed in the following subsection. Once the required load and actuator displacement was determined, the girder was unloaded, and the loading was repeated for a total of 1000 load-unload cycles. The loading rate was set at 2 cycles/min for the first 100 cycles, before being increased to 4 cycles/min for the remaining 900 cycles.

**(a)**

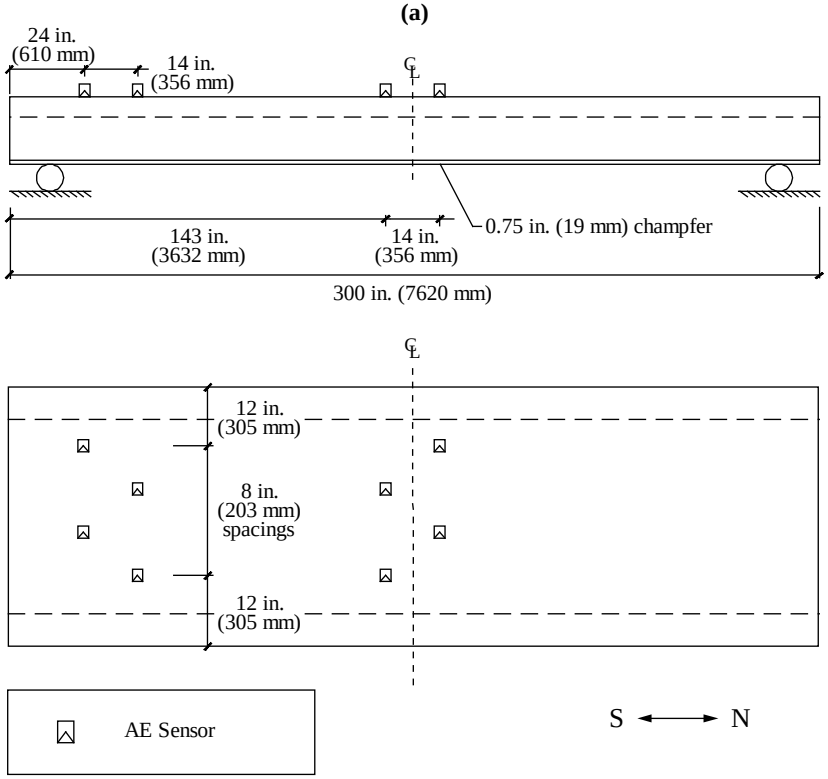


**(b)**

**Figure 26. (a) AE sensor and (b) placement of AE sensors.**

After addition of the UHPC overlay, girder H-PS-C-300-R-UO was subjected to a second cyclic loading sequence, herein referred to as Cyclic Loading 2 (CL2). The same loading sequence and load rates employed for CL1 were repeated for CL2.

Deflection Criteria for Cyclic Loading: The loading sequence employed for cyclic loading (CL1 and CL2) of girder H-PS-C-300-R-UO was selected to produce a mid-span deflection based on the criteria outlined below and summarized in Table 12. It was determined that cyclic loading would be applied to a mid-span deflection of 0.400 in. (10.2 mm) to encompass all criteria.

1. Criteria for deflections as outlined by AASHTO 2.5.2.6.2 *(33)*. The criterion selected states an allowable deflection limit for general vehicular load on concrete bridges equal to Span/800. For the clear span of 288 in. (7315 mm) used for testing, the allowable deflection limit was calculated to be 0.360 in. (9.14 mm).
2. Application of design truck as outlined by AASHTO 3.6.1.2.2 *(33)*. Regarding the characteristics of the design truck provided in Figure 27, the 72-in. (1830 mm) transverse spacing of wheels results in only a single wheel load of each axle present on the 48-in. (1220-mm) width of girder H-PS-C-300-R-UO. Thus, a distribution factor of one (DF = 1.0) was conservatively assumed for the following two configurations:
    a. To produce extreme force effect, the 32.0-kip (142-kN) axles were assumed to be spaced at 14.0 ft. (4.27 m), with one 16-kip (71.2-kN) wheel load per axle placed on the girder equidistant from mid-span. The mid-span deflection due to this configuration was calculated to be 0.228 in. (5.80 mm).
    b. The total force of a single 32.0-kip (142-kN) axle was assumed to act as a point load at mid-span. The mid-span deflection due to this configuration was calculated to be 0.388 in. (9.85 mm).

**Table 12. Summary of deflection criteria for cyclic loading.**

| Case | Load | Criterion | Description | Deflection in. (mm) |
|---|---|---|---|---|
| **1** | Span/800 | AASHTO 2.5.2.6.2 | Girder clear span of 288 in. (7315 mm) | 0.36 (9.14) |
| **2a** | Design Truck | AASHTO 3.6.1.2.2 | 16.0-kip (71.2-kN) axles spaced 14.0 ft. (4.27 m) and positioned equidistant from girder mid-span | 0.23 (5.79) |
| **2b** | Design Truck | AASHTO 3.6.1.2.2 | 32.0-kip (142-kN) point load at girder mid-span | 0.39 (9.86) |
| | | | Cyclic Loading Target Deflection | 0.4 (10.16) |

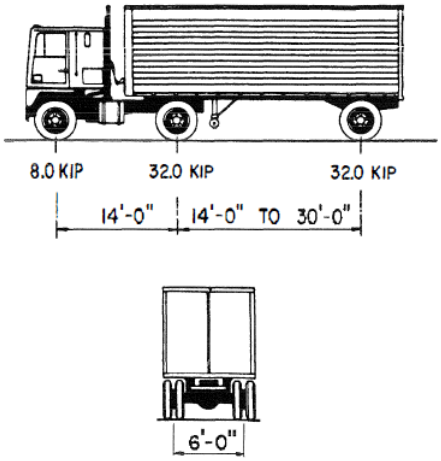


**Figure 27. Characteristics of the design truck *(33)*.**

### *4.11.4. Ultimate Loading*

Ultimate loading of girder H-PS-C-300-R-UO in longitudinal four-point bending began with a series of four, deflection based cyclic loadings. The girder was loaded to a mid-span deflection of 1.0 in. (25.4 mm) at 0.25-in. (6.35-mm) increments, for a total of four increments. At each increment, the girder was cycled (i.e., loaded and unloaded) three times. A constant load rate of 0.05 in./min (1.27 mm/min) was used for the first increment, then increased to 0.10 in./min (2.54 mm/min) for the remaining three. Girder H-PS-C-300-R-UO was then loaded in 1.0-in. (25.4-mm) increments at 0.10 in./min (2.54 mm/min) to a final, ultimate load and deflection.

# 5. FINDINGS

## 5.1. Compressive Strength

### *5.1.1. Slant-Shear*

Table 13 presents the average compressive strengths obtained from 3.94 in. (100 mm) cube specimens cured at ambient conditions (68°F [20°C] and 30% relative humidity). These results are plotted in Figure 28 to illustrate the strength gain versus time. The minimum 28-day strength required by ASTM C1856 is 17,000 psi (20 MPa) *(6)*. By that definition, the concrete mixture used in this research qualifies as UHPC.

**Table 13. Compressive strength results for UHPC in psi (MPa).**

| 1 day | 3 days | 7 days | 28 days |
|---|---|---|---|
| 3580 | 11,060 | 14,660 | 17,220 |
| (24.7) | (76.3) | (101.1) | (118.8) |

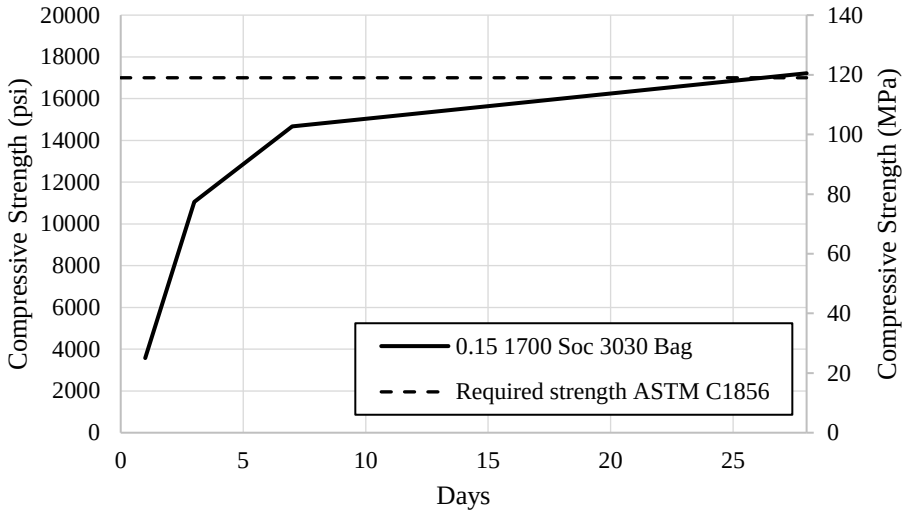


**Figure 28. Compressive strength results for UHPC.**

## 5.2. Bond Strength

### *5.2.1. Slant-Shear*

Table 14 and Figure 29 present the average bond strengths from the slant-shear tests conducted seven days after the UHPC overlay was applied. ACI recommends a bond strength for repair concrete of 1000 psi (7 MPa) *(22)*. The data show that regardless of the texture depth, shear strengths of the bonded interface were greater than the required strength. However, greater bond strengths were achieved from textures that provided greater interlocking such as the rough texture, horizontal grooves, and diagonal/cross-hatch grooves. These results are promising because even in the case of a light grinding texture depth of 0.002 in. (0.05 mm) the minimum bond strength was achieved.

**Table 14. Slant-shear bond strengths.**

| **Texture (in [mm])** | **Ave. Shear Stress** psi [MPa] | **Ave. Normal Stress** psi [MPa] | **Shear Standard Deviation** psi [MPa] |
|---|---|---|---|
| Lightly Ground (0.002 [0.05]) | 1032.1 [7.1] | 1191.8 [8.2] | 266.3 [1.8] |
| Horizontal Grooves (0.035 [0.9]) | 1744.0 [12.0] | 2013.8 [13.9] | 253.5 [1.7] |
| Diagonal Grooves Cross-Hatch (0.063 [1.6]) | 1735.6 [12.0] | 2004.1 [13.8] | 151.2 [1.0] |
| Diagonal Grooves @45° (0.063 [1.6]) | 1654.5 [11.4] | 1910.4 [13.2] | 106.8 [0.7] |
| Vertical Grooves (0.063 [1.6]) | 1416.1 [9.8] | 1635.1 [11.3] | 137.7 [0.9] |
| Rough (0.11 [2.8]) | 2873.7 [19.8] | 3318.3 [22.9] | 387.6 [2.7] |

### *5.2.2. Splitting Tension*

Table 15 and Figure 30 present the results from the split-cylinder and split-prism tests conducted seven days after the UHPC overlay was applied. ACI recommends a tensile strength for repair concrete of 150 psi (1 MPa) *(22)*.

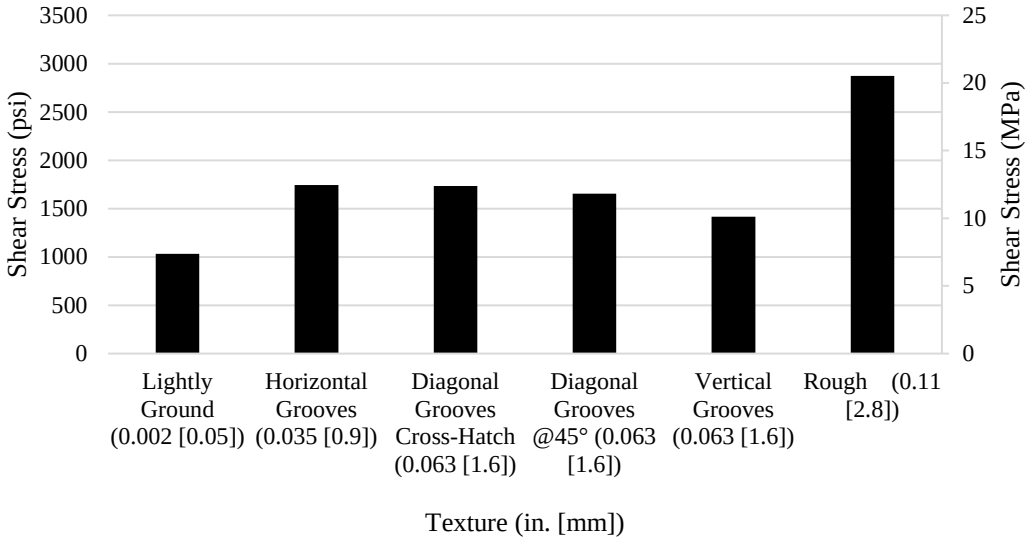


**Figure 29. Slant-shear bond strengths.**

**Table 15. Splitting tension strengths.**

| **Splitting Tensile Strength (psi [MPa])** | **Lightly Ground Texture** 0.002 in. [0.05 mm] | **Horizontal Grooved Texture** 0.035 in. [0.9 mm] | **Horizontal Grooved Texture** 0.063 in. [1.6 mm] | **Rough Texture** 0.11 in. [2.8 mm] |
|---|---|---|---|---|
| Cylinders | 253.9 [1.8] | 305.5 [2.1] | 243.9 [1.7] | 351.1 [2.4] |
| Standard Deviation | 46.8 [0.32] | 103.9 [0.72] | 45.2 [0.31] | 140.1 [0.97] |
| Prisms | 224.7 [1.5] | 389.1 [2.7] | 464.1 [3.2] | 538.3 [2.7] |
| Standard Deviation | 69.6 [0.48] | 105.6 [0.73] | 104.2 [0.72] | 74.0 [0.51] |

Table 15 and Figure 30 show that the bond strength of composite, cylindrical specimens did not correlate well with texture depth. However, the bond strength of prismatic specimens appeared to be strongly influenced by texture. The data show that there was a wide disparity between splitting tensile strengths from 225 psi to 538 psi (1.5 MPa to 3.7 MPa). This can be attributed to the greater surface area available for bonding provided by the more textured surfaces. It is also important to note that all of the bond strengths from cylindrical and prismatic specimens were greater than the required minimum strength for direct tension testing (150 psi [1 MPa]) regardless of texture depth. Again, the results are promising because even in the case of a light grinding texture depth of 0.002 in. (0.05 mm) the minimum bond strength was achieved.

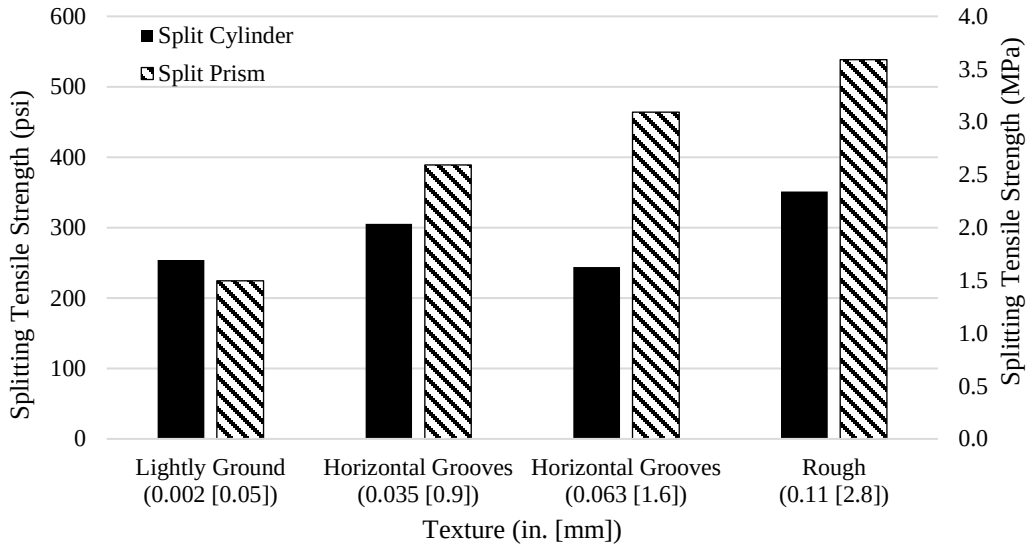


**Figure 30. Splitting tension strengths.**

### *5.2.3. Direct Tension*

Table 16 and Figure 31 present the results from the direct tension tests conducted seven days after the UHPC overlay was applied. ACI recommends a tensile strength for repair concrete of 150 psi (1 MPa) *(22)*. As shown in Table 16, the surface texturing by grinding had tensile strengths that were below 150 psi and, therefore, did not meet minimum requirements. However, surfaces prepared by chipping provided sufficient bond strengths on average.

**Table 16. Direct tensile strengths.**

| | **Horizontal Grooved Texture** 0.035 in. [0.9 mm] | **Chipped Texture** 0.04 in. [1.0 mm] | **Rough Texture** 0.11 in. [2.8 mm] |
|---|---|---|---|
| Average Tensile Strength (psi [MPa]) | 63.8 [0.44] | 153.7 [1.06] | 139.2 [0.96] |

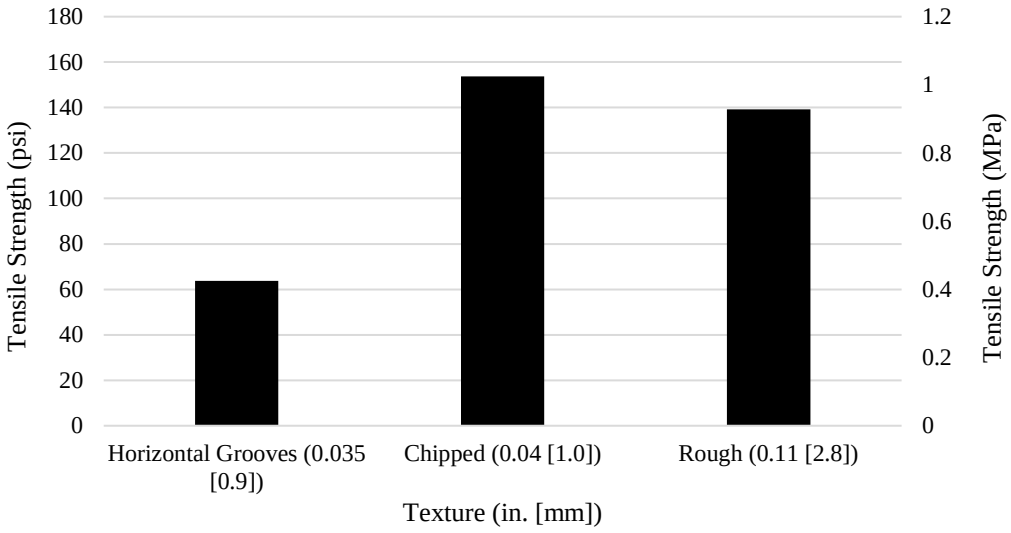


**Figure 31. Direct tension strengths.**

The data show that type of texture greatly affected the tensile strength developed. All of the horizontal grooves specimens had strengths less than 1 MPa, which is very low and unacceptable. However, one of the specimens displayed a substrate failure (Figure 32) indicating that the observed strengths may have been limited by the tensile strength of the immature substrate. Rough and chipped textures had greater strengths than the grooved texture achieved by grinding that can be attributed to greater surface area and exposure of aggregate and pores that allowed UHPC to bond more easily. However, the rough texture still did not provide adequate strength (less than 150 psi [1 MPa]).


**Figure 32. Substrate failure in direct tension specimen.**

To investigate the cause of the low strengths, chipping was used to produce a substrate with a minimally acceptable texture of 0.04 in. (1 mm) that was selected based on observations by Harris et al. *(37)*. The acceptable bond strength of the chipped specimens seems to indicate that grinding plugs pores that are essential for bond of the overlay. It is also important to note that results of from the rough and chipped textures are considered "fair" according to similar work performed by Sprinkel and Ozyldirim *(38)*.

Most importantly, it should be noted that the minimum acceptable texture depth under field conditions is 0.25 in. (6.35 mm) *(22)*. Since all of the bond assessment tests were able to produce adequate bond strengths with textures less than 0.08 in. (2 mm), the results are particularly attractive.

## 5.3. Shrinkage and Temperature Effects

### *5.3.1. Early-Age Shrinkage*

The early-age shrinkage test was conducted on a 6x6x24 in. (152x152x610 mm) UHPC beam. Figure 33 presents the early-age shrinkage results collected for the full seven days at 15-second increments. The total shrinkage strain during this period was approximately 1800 μstrain. Figure 34 presents the results from the first 24 hours, during which the total shrinkage strain was approximately 1400 μstrain. It is difficult to establish set times for UHPC mixtures because they can be extremely viscous in the fluid state. By stripping molds at early ages and watching for slumped specimens, the set time for the UHPC mixture is estimated to be 10 hours. During the first 10 hours, the UHPC is in a plastic state that may not transfer shear stress to the substrate concrete. Consequently, it appears that although the early-age shrinkage is substantial, approximately 55% (roughly 1000 μstrain) of it occurs in the plastic state and may not contribute to bond stresses since the elastic modulus of the UHPC should be small at such early ages.

Similar early-age shrinkage tests conducted by *(10)* produced the results shown in Figure 35. The magnitude of the shrinkage strains at 24 hours is comparable to those observed in this study.

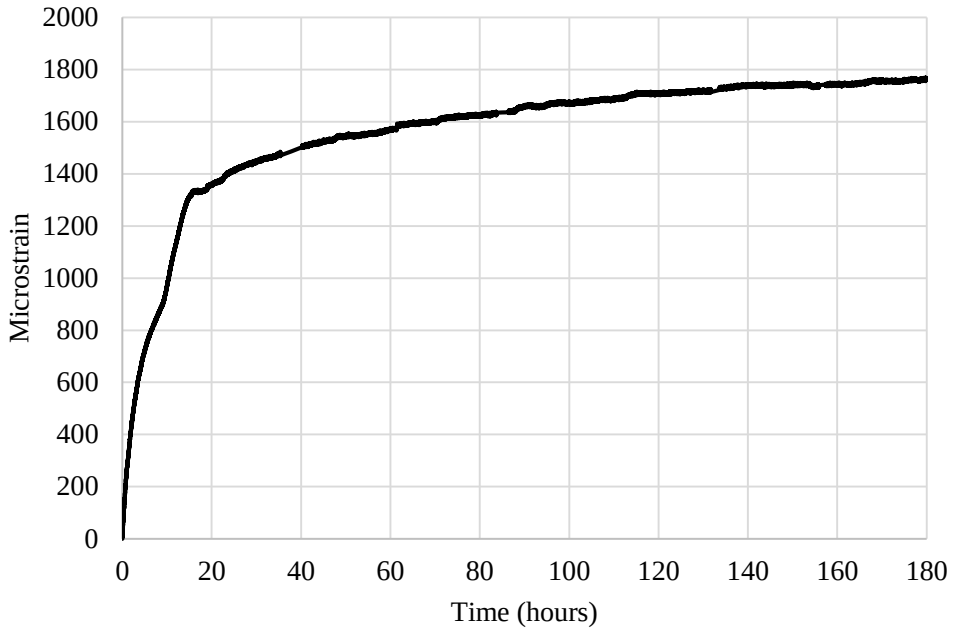


**Figure 33. Early-age shrinkage data over seven days.**

### *5.3.2. Longer-Term Shrinkage*

The longer-term shrinkage testing was conducted on 3x4x16 in. (76x102x406 mm) UHPC prisms. The test was conducted for 28 days taking readings using a comparator once a day.

Figure 36 shows the results of the longer-term shrinkage test. The specimens were cured for 7 days in the wet room then taken out and cured in ambient conditions for the remainder of the test. As seen in the plot, the shrinkage plateaus around 4 days. The shrinkage resumed once the specimens were exposed to drying. The shrinkage begins to plateau around 20 days at about 450 microstrain.

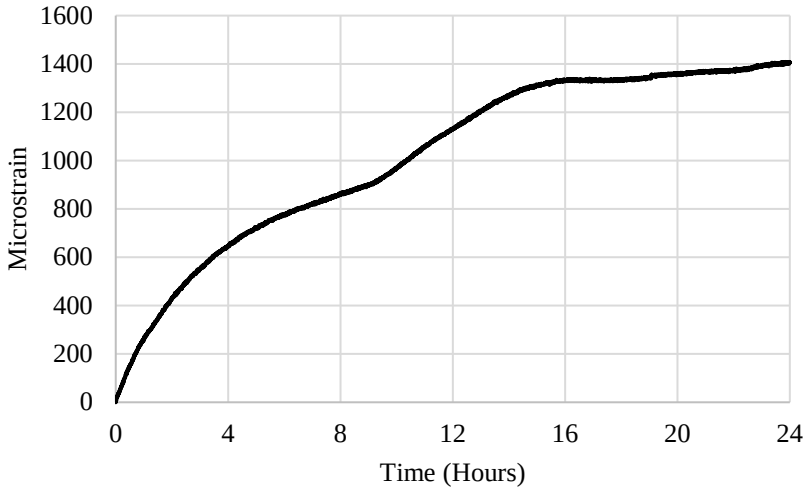


**Figure 34. First 24 hours of early-age shrinkage data.**

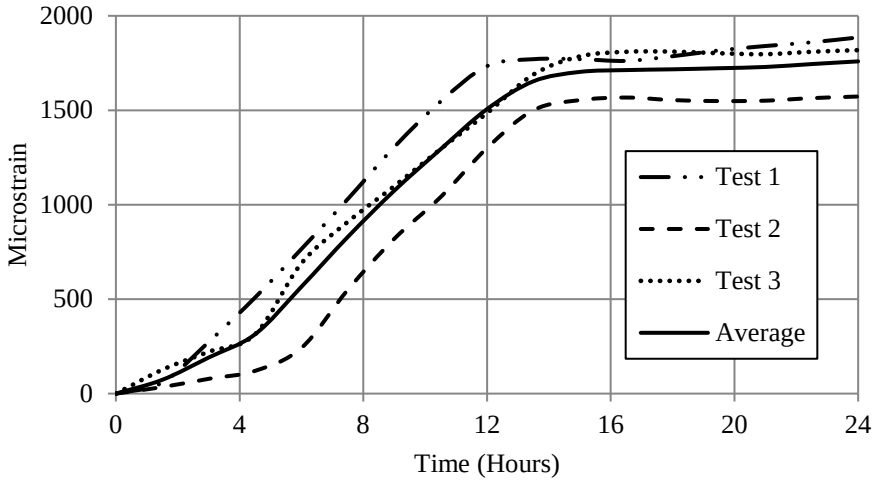


**Figure 35. Early-age shrinkage results *(10)*.**

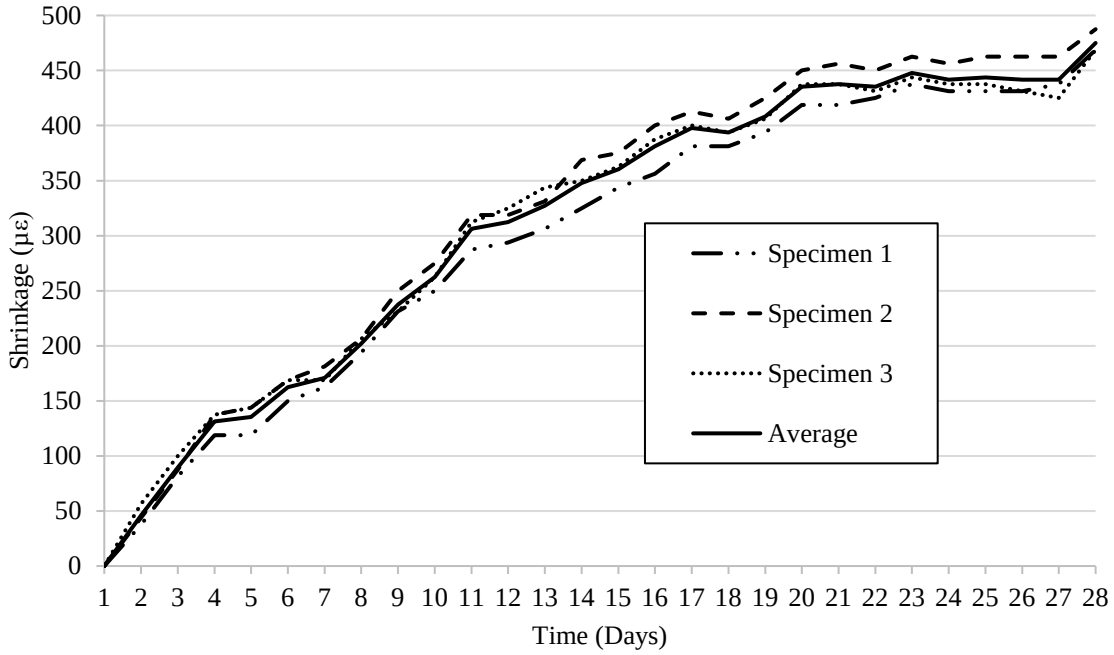


**Figure 36. Longer-term shrinkage data.**

### *5.3.3. Coefficient of Thermal Expansion*

The coefficient of thermal expansion test was conducted on 3x4x16 in. (76x102x406 mm) UHPC prism specimens in accordance to Tex-428-A *(21)*.

The coefficient of thermal expansion test resulted in a coefficient of thermal expansion value of 10.8 μ/°F (19.5 μ/°C). This value is about 60% greater than what would be commonly expected for NSC concrete (typically near 5.5 μ/°F [10 μ/°C]), indicating that the thermal

movements of the UHPC overlay will be substantially greater than the substrate concrete that will typically have a lower coefficient of thermal expansion and also experience smaller temperature swings.

## 5.4. Rapid Chloride Permeability Tests

RCPTs were conducted on two specimens, one was fiber reinforced and the other was non-fiber reinforced. The tests were conducted for a total of 6 hours with measurements taken every 30 minutes. Results from these tests are presented in Table 17.

The results show that in both cases a negligible charge passed through specimens over the period that voltage was applied. A total charge of 0.96 coulombs and 1.08 coulombs were observed for fiber reinforced and non-fiber reinforced specimens, respectively. The negligible charge can be attributed to the high density of UHPC that may have limited saturation when specimens were submerged in deionized water and discontinuity in the UHPC capillary pores. Additionally, fiber reinforcement tends to be discontinuous, which can prevent significant charge from passing through specimens. The results of chloride permeability testing are important to some transportation agencies as an indication of UHPC's ability to improve durability against deicing salts that can cause corrosion of steel fibers or reinforcement.

The charge passed during the RCPTs is extremely low and indicates that the UHPC specimens behaved nearly the same as insulators. The authors are confident that the test was performed correctly and this behavior is attributed to the fact that the UHPC specimens used for the RCPT were allowed to dry cure to an age of 56 days prior to preparing them for the RCPT according to ASTM C1202. It should be noted that other researchers have obtained greater passed charge numbers for other UHPC mixtures. Several researchers *(39-42)* have shown that UHPC specimens that have been wet (or steam) cured continuously prior to testing generally produce a passed charge of 5 to 25 coulombs. Air-cured specimens tested by Ahlborn et al. *(39)* had an average passed charge of 75 coulombs.

**Table 17. RCPT results.**

| Specimen | Charge passed (coulombs) |
|---|---|
| Fiber reinforced | 0.963 |
| Non-fiber reinforced | 1.08 |

## 5.5. Slab Tests

### *5.5.1. Principal Characteristics*

To better understand the temperature and shrinkage behavior of slabs, principal characteristics of UHPC and NSC were compared such as compressive strength, modulus of elasticity, and flexural performance. Table 18 shows the material properties for both the NSC and UHPC. Due to the small volumes of the UHPC batches, companion specimens were not available for each batch. The UHPC mix design was the same for all the batches; thus, results were expected to be similar for each batch. Although some of the compressive strengths presented in Table 18 are less than the 17,000 psi (120 MPa) required for UHPC, these data represent only a small fraction of total number of samples tested for these mixture proportions.

**Table 18. Comparison of principal characteristics of NSC and UHPC.**

| Specimen | Modulus of Elasticity ksi (MPa) | Compressive Strength ksi (MPa) | Flexural Performance: Ultimate Load lbs. (N) | Flexural Performance: First Peak Load lbs. (N) | Modulus of Rupture: First Crack psi (MPa) |
|---|---|---|---|---|---|
| **Specimen 1 (NSC)** | 3,686 (25,414) | 5.33 (36.71) | 3,270 (14,546) | 3,270 (14,546) | 817.5 (5.64) |
| **Specimen 2 (NSC)** | - | 5.39 (37.16) | 2,970 (13,211) | 2,970 (13,211) | 742.5 (5.12) |
| **Slab 1 (UHPC)** | - | 15.83 (109.14) | 8,990 (39990) | 7,636 (33,967) | 1,909 (13.16) |
| **Slab 2 (UHPC)** | - | - | - | - | - |
| **Slab 3 (UHPC)** | - | 17.85 (123.04) | - | - | - |
| **Slab 4 (UHPC)** | 6,147 (42,382) | 16.75 (115.47) | - | - | - |
| **Slab 5 (UHPC)** | - | 17.8 (122.72) | 8,970 (39,901) | 7,706 (34,278) | 1,927 (13.29) |

The temperature experienced by the slabs was recorded with the VWSGs and compared with the temperature recorded by the National Weather Service in Las Cruces, New Mexico. The temperatures measured by both sources are similar, with slightly higher temperatures measured in the slabs. This difference can be attributed to the slabs being placed in a location with minimal shade throughout the day. Therefore, the slabs have a complete exposure to sunlight during peak temperatures. Figure 37 shows the temperature record for Las Cruces, New Mexico and Figures 38 to 42 show the temperatures measured in Slabs 1-5, respectively. Each slab has four VWSGs. The naming convention used is: VSTL - Vibrating Wire Strain Gauge in the Top Left side, VSBL - Bottom Left, VSTR - Top Right and VSBR - Bottom Right. It should be noted that left and right were defined at the time of casting. Figures 38 and 39 (Slabs 1 and 2) have a gap in the data from 55 to day 76 due to power loss to the datalogger. Also, these two slabs show less fluctuation in temperature after day 52 when the slabs were moved inside the laboratory with controlled conditions. Figures 40 to 42 (Slabs 3-5) show similarities in temperature measurements, as expected with only slight variations due to differences in thickness.

The National Weather Service temperature measurements in Las Cruces, New Mexico from February to June 2018 had average temperatures varying from 50°F (10°C) to 86°F (30°C), with a maximum temperature of almost 104 °F (40.0°C) and a minimum temperature of almost 32°F (0°C). These temperatures were similar to the ones registered by the VWSGs in the slabs, which had average temperatures ranging from 40°F (4.4°C) to 122°F (50.0°C), with a maximum temperature of 140°F (60.0°C) in the slabs exposed to environmental conditions and a minimum temperature of approximately 32°F (0°C).

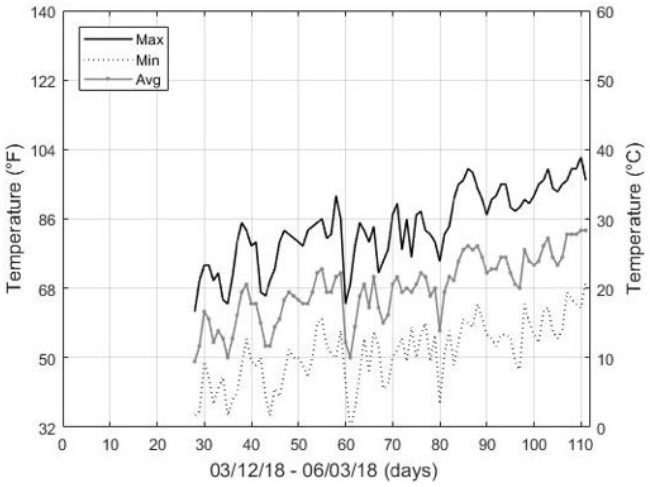


**Figure 37. Temperature in Las Cruces, NM.**

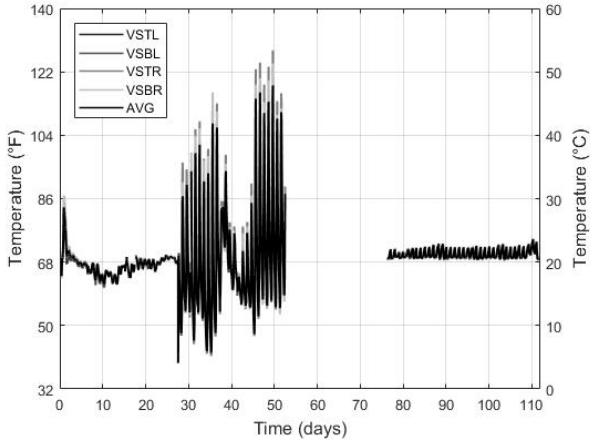


**Figure 38. Temperature changes in Slab 1.**

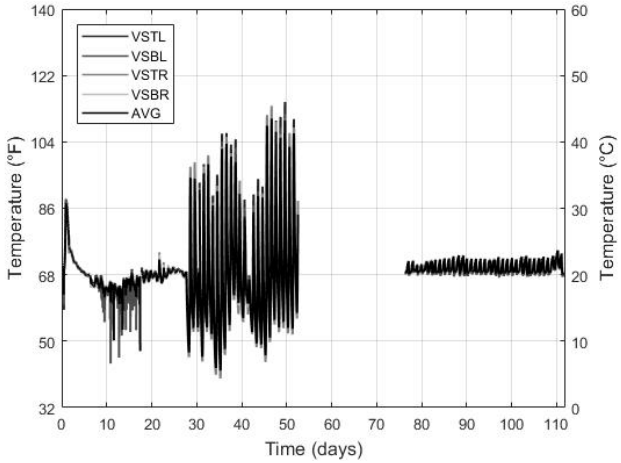


**Figure 39. Temperature changes in Slab 2.**

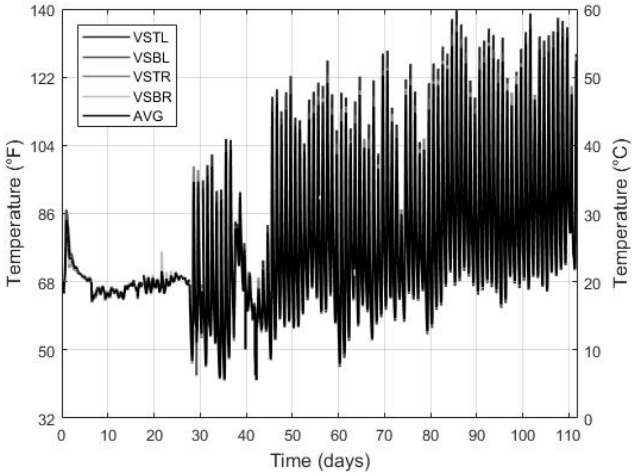


**Figure 40. Temperature changes in Slab 3.**

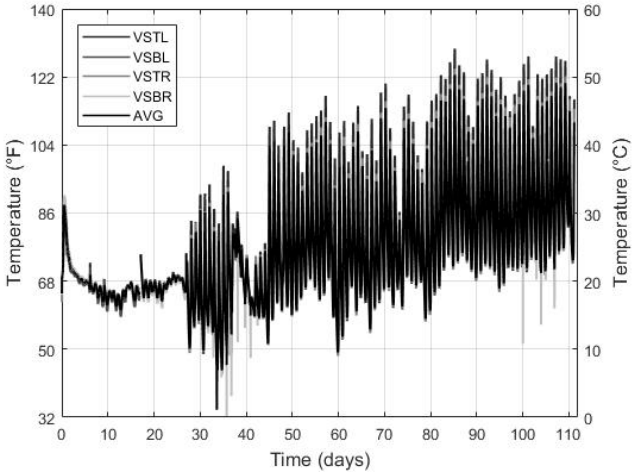


**Figure 41. Temperature changes in Slab 4.**

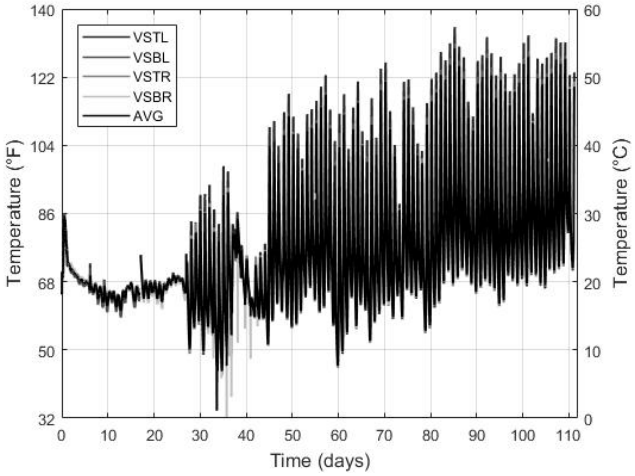


**Figure 42. Temperature changes in Slab 5.**

Figures 43-47 show the strain versus time plots for Slabs 1-5, respectively. Annotations of the principal events that the slabs experienced from the casting day until the last recorded data day are noted on the Figures. A jump in strain occurred at day seven when the formwork was removed. At day 27, the slabs were exposed to environmental conditions (moved from inside the laboratory to outdoors) to prepare for the overlay placement. The environmental change at day 27 caused the strain to experience more fluctuation due to greater changes in temperature. At day 37, when the deck was placed, the sensors near the top of the slabs started having smaller strain values (around -200 με), and the sensors at the bottom recorded greater strain magnitudes, around -350 με. This behavior is attributed to wet curing procedures, which appear to have caused the top sensors to experience less strain near locations where the surface was wetted. The wet surface can induce expansion of the material, and the bottom sensors are less sensitive to the moisture conditions of the top surface. The last event that Slabs 1 and 2 were subjected to was the controlled exposure (these slabs were moved back into the laboratory). Due to the controlled temperature in the laboratory, fluctuations in temperature, and subsequently strain, was dramatically reduced.

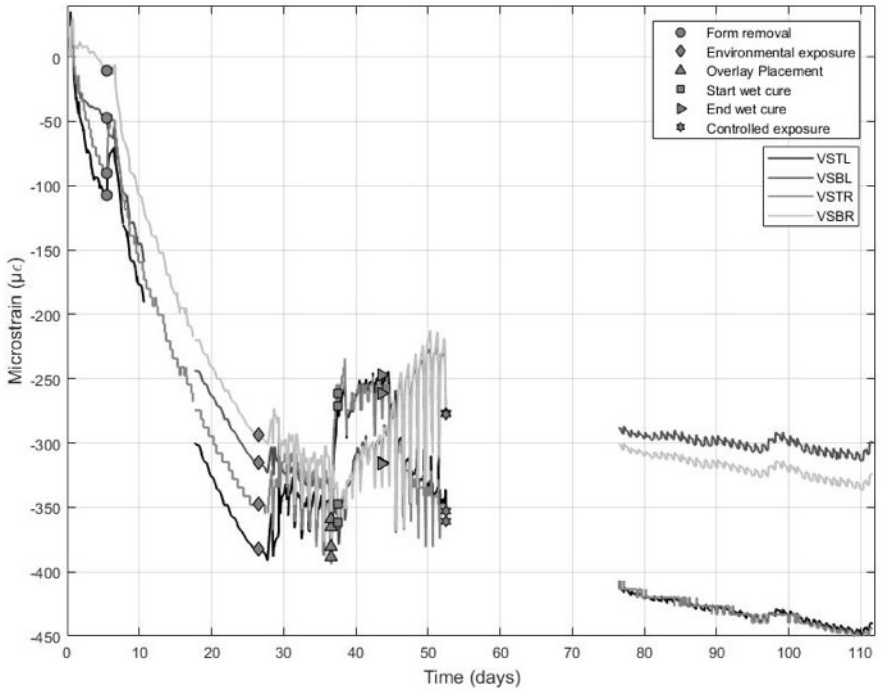


**Figure 43. Strain versus time in Slab 1.**

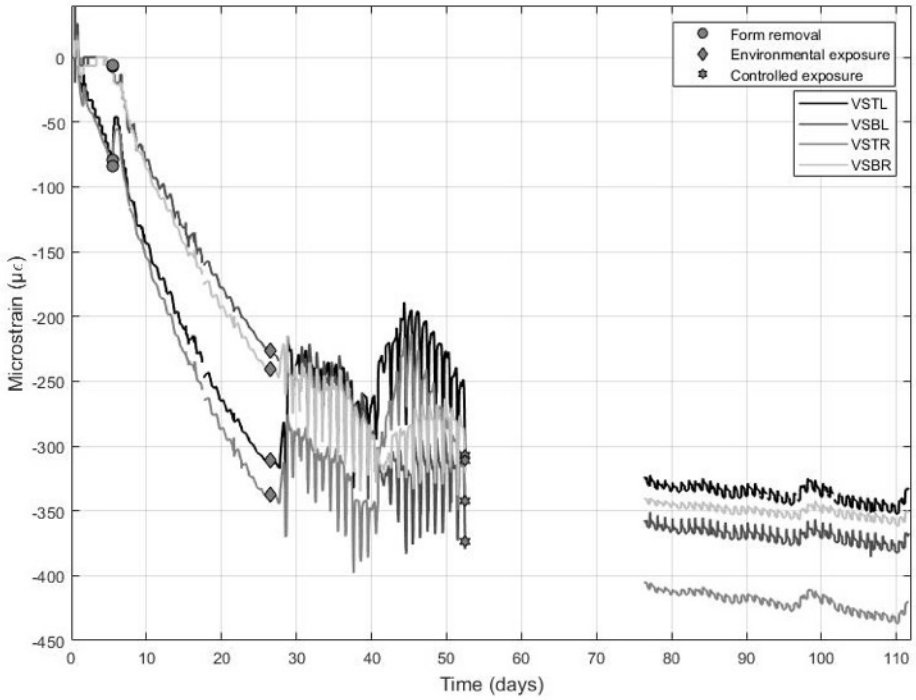


**Figure 44. Strain versus time in Slab 2.**

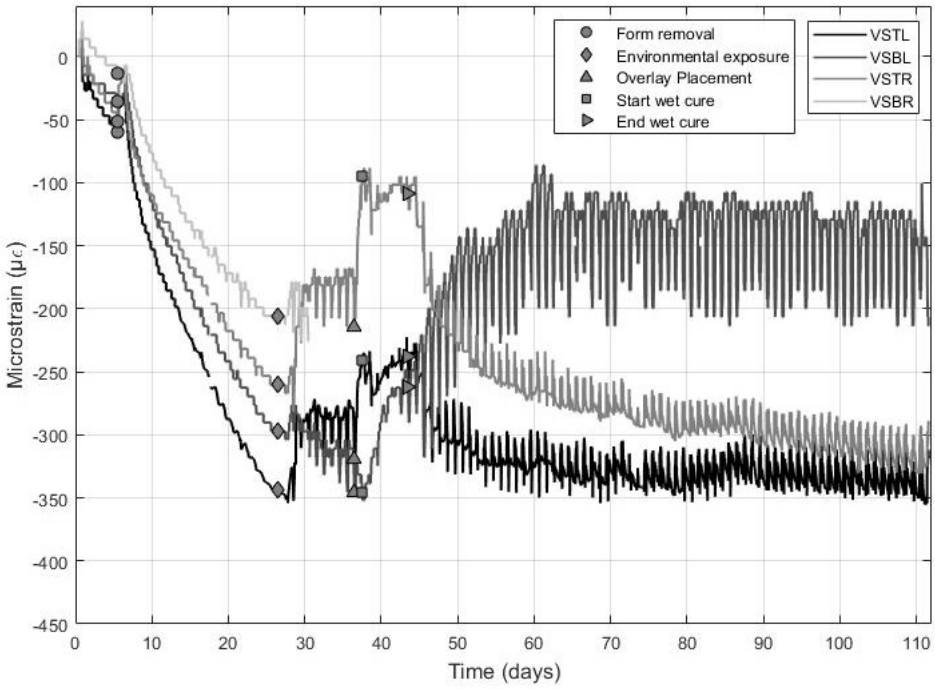


**Figure 45. Strain versus time in Slab 3.**

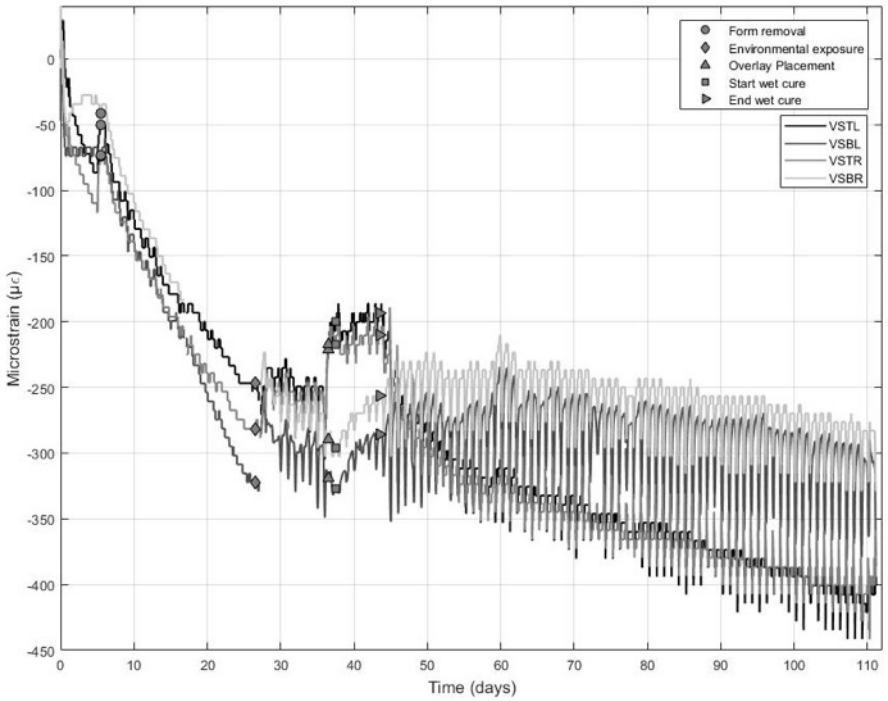


**Figure 46. Strain versus time in Slab 4.**

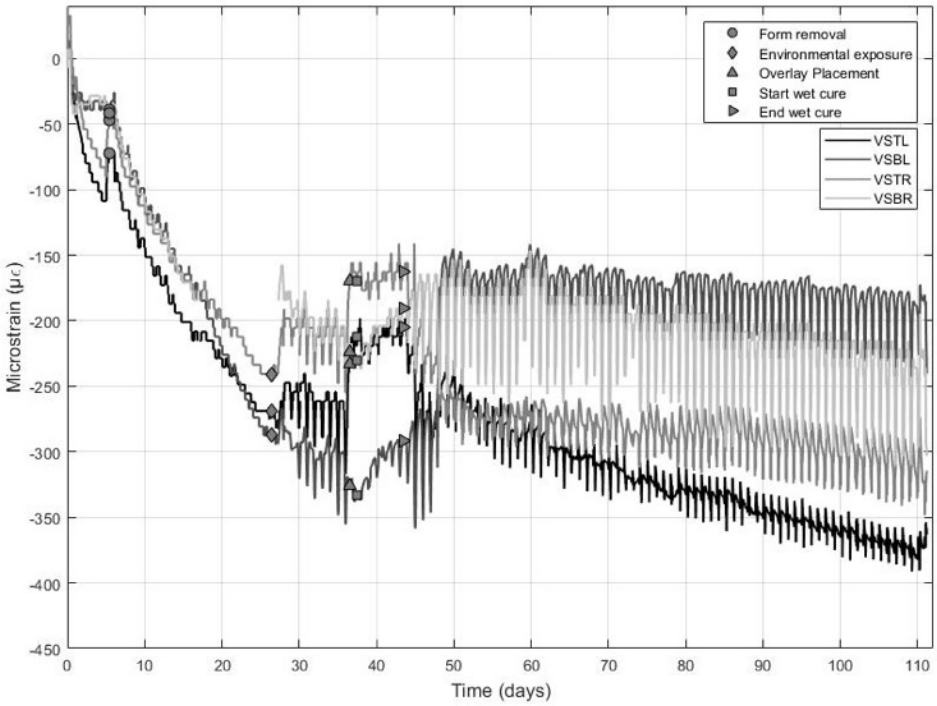


**Figure 47. Strain versus time in Slab 5.**

The first pair of slabs to be compared are Slab 1 and Slab 2. Both slabs have a NSC substrate thickness of 4 in. (102 mm), a reinforcement mesh of No. 3 (No. 10) bars, and were kept in controlled conditions. The difference between the two specimens is that Slab 1 has a UHPC

overlay and Slab 2 does not have an overlay. In general, the strains measured in the two slabs followed the same trend up to the placement of the overlay on Slab 1. At that point, the average strains were -373.4 με and -317 με for Slabs 1 and 2, respectively, with the top and bottom gauges measuring similar values. After the placement of the UHPC overlay, the strain gauges (VSTL and VSTR), near the top of the slab decreased in value due to the compressive force induced by shrinkage of the overlay. The strain gauges (VSBL and VSBR) near the bottom of the slab experienced an increased rate of tensile strain due to the bending effect created by the eccentric load produced by shrinkage of the UHPC overlay. This is in contrast to the trends observed in Slab 2 (no overlay). The strains measured in Slab 2 continued to increase more uniformly with the top and bottom gauges measuring similar strains. It is noted that the strains measured during the period when the overlay was wet cured (day 37 to day 43) were influenced by the curing. During this period, the changes in strain remained small, particularly near the top of the slabs were moisture was applied.

The next pair of specimens to be compared is Slab 3 (Figure 45) and Slab 4 (Figure 46). These slabs have a reinforcement mesh made of No. 4 (No. 13) bars, a 1 in. (25.4 mm) thick UHPC overlay, and were exposed to environmental conditions. The different parameter in these slabs was the thickness of the NSC substrate. Slab 3 had a substrate thickness of 4 in. (102 mm) and Slab 4 had a substrate thickness of 6 in. (152 mm). As shown in Figure 46 (Slab 4) the strain was approximately 22% greater than the measured strain in Slab 3 (Figure 45), and the strains for Slab 4 measured on top and bottom were more similar to each other than the strains measured in the top and bottom of Slab 3. The greater strains in Slab 4 were unexpected because the thicker substrate was expected to restrain shrinkage in the overlay. It is possible that because the overlay on Slab 3 was closer to the reinforcement, the reinforcement provided more restraint than the thicker substrate of Slab 4.

Comparing Slab 3 (Figure 45) and Slab 5 (Figure 47), both slabs have a 4 in. (102 mm) thick NSC substrate, a 1 in. (25.4 mm) thick UHPC overlay, and were exposed to environmental conditions. The difference between this pair of slabs was that Slab 3 had a mesh of No. 4 (No. 13) bars and Slab 5 has a mesh of No. 3 (No. 10) bars. The strain changes in Slab 5 (Figure 47) tend to be more similar in the top and bottom sensors than the strains measured in Slab 3 (Figure 45). However, the measured strains were greater in the substrate that contained the smaller reinforcement ratio (Slab 5).

The last pair of slabs that was compared was Slab 1 (Figure 44) and Slab 5 (Figure 47). Both slabs had a 4 in. (102 mm) thick NSC substrate, a 1 in. (25.4 mm) thick UHPC overlay, and reinforcement mesh consisting of No. 4 (No. 13) bars. The difference between these two slabs was that Slab 1 was exposed to controlled conditions and Slab 5 was exposed to environmental conditions. As expected, the measured strains in Slab 1 became more uniform after being placed in controlled conditions, having less fluctuation in the strain and temperature measurements.

Figure 48 shows the average change in dimensions for each slab. Prior to being moved outside, Slab 1 experienced the greatest change in length, approximately -0.06 in. (1.5 mm). Once they were exposed to the environment, Slab 1 and Slab 2 experienced similar shrinkage. The slabs

with the least amount of shrinkage were Slab 3 and Slab 5 with changes in length of approximately -0.04 in. (-1.0 mm).

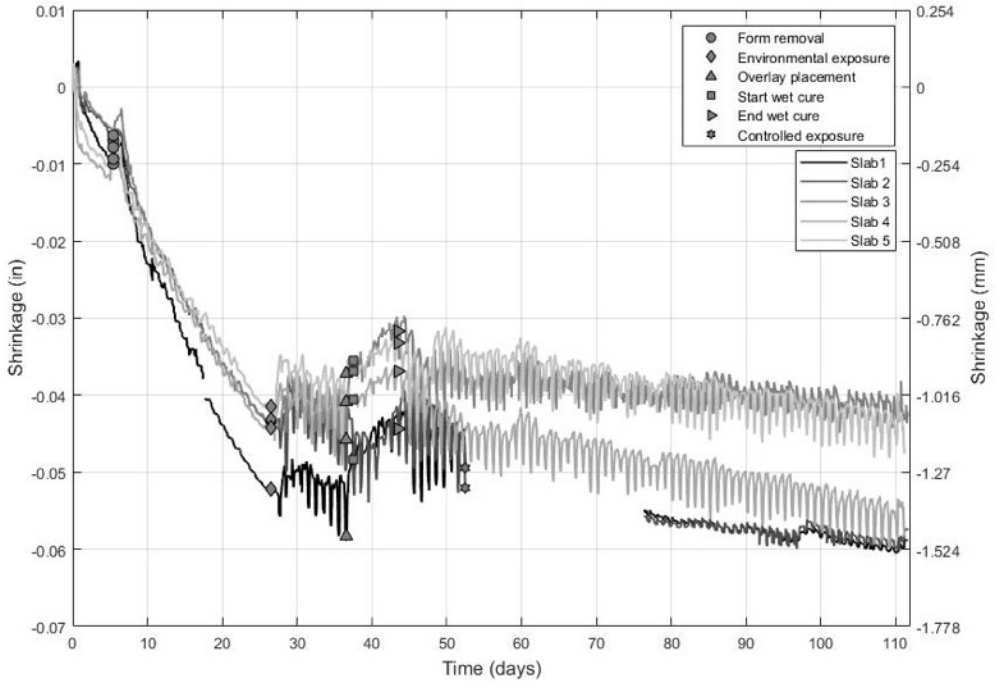


**Figure 48. Shrinkage versus time.**

In Figure 49, the strains due to each UHPC overlay were isolated from the total strain measured in the slabs by subtracting the average strain at the time of overlay placement. Isolation of the strains caused by the overlay were desired to compare the impact that the UHPC overlay had on each NSC substrate. As can be seen in Figure 49, Slab 3 experienced less shrinkage due to the UHPC overlay. This can be attributed to the increased reinforcement in the substrate that should be expected to restrain shrinkage.

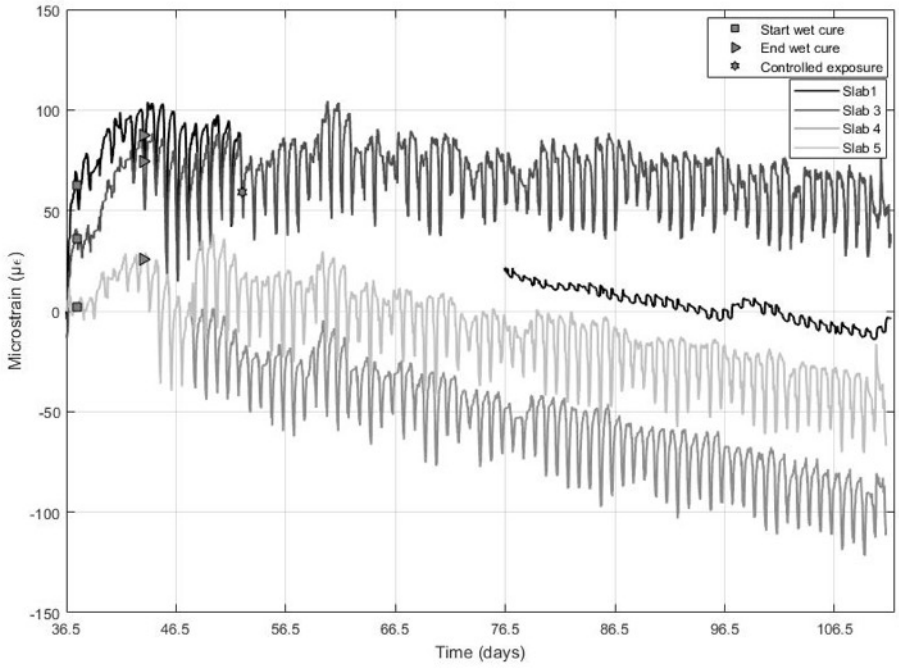


**Figure 49. Shrinkage due to UHPC overlay.**

To isolate the strain caused by the overlay, the average shrinkage strain of the substrate at day 36.5 (immediately prior to the application of the overlay) was subtracted from the total strain. Figures 50-53 show the strains from day 36.5 onward, with the average strain developed in the substrate subtracted from the total strain. This strain includes strain caused by shrinkage of the overlay plus any shrinkage strains developed in the substrate. To eliminate the strain developed from the shrinkage of the substrate, the average strain developed in Slab 2 (with no overlay) was also subtracted from the total strain. Close inspection of the strains indicates that wet curing the overlay for approximately seven days influenced the behavior of the slabs between days 38-45. Therefore, the influence of the shrinkage of the overlay is presented from day 50.5 onward to avoid the effects of curing.

Figures 54-57 show the strain developed in the substrate due to shrinkage of the UHPC overlay. These data were used to develop a best fit line and equation (3rd order polynomial). Strains from the polynomial equation were used to calculate the neutral axis height assuming a linear strain distribution through the thickness of the substrate. It is noted that this produces an approximate neutral axis height. The neutral axis height was estimated as:

$$NA = \frac{x\,\epsilon_b}{\epsilon_t - \epsilon_b} + y \qquad [9]$$

where:
NA = neutral axis height,
$\epsilon_t$ = strain average of top VWSGs,
$\epsilon_b$= strain average of bottom VWSGs,
x = distance from bottom VWSGs to top VWSGs, and
y = distance from the bottom of the slab to the bottom VWSGs.

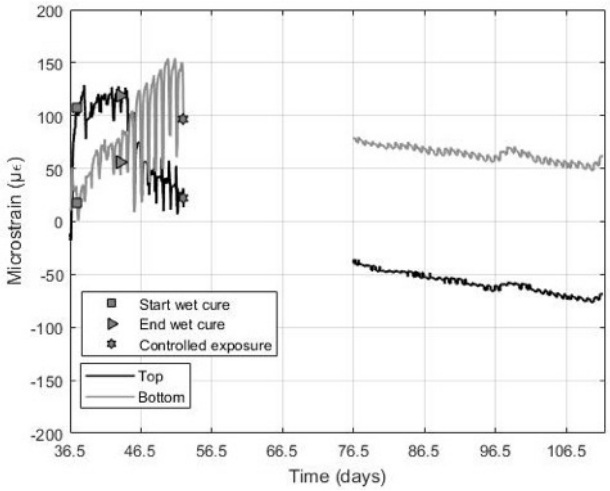


**Figure 50. Strain versus time isolating UHPC for Slab 1.**

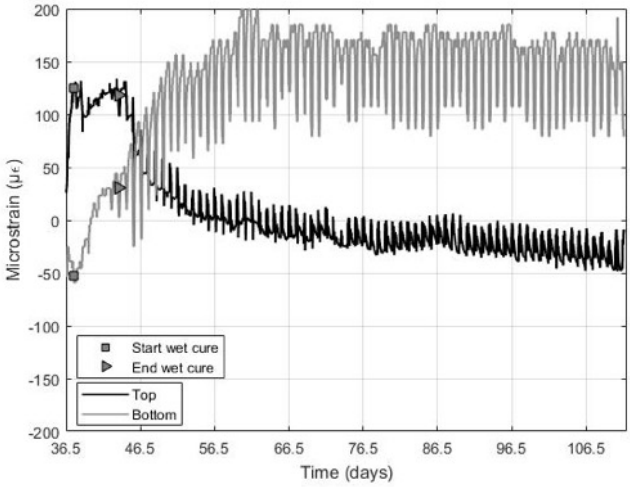


**Figure 51. Strain versus time isolating UHPC for Slab 3.**

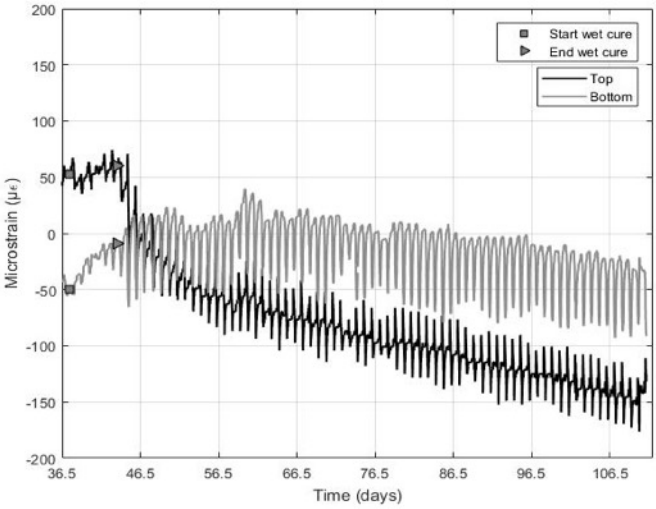


**Figure 52. Strain versus time isolating UHPC for Slab 4.**

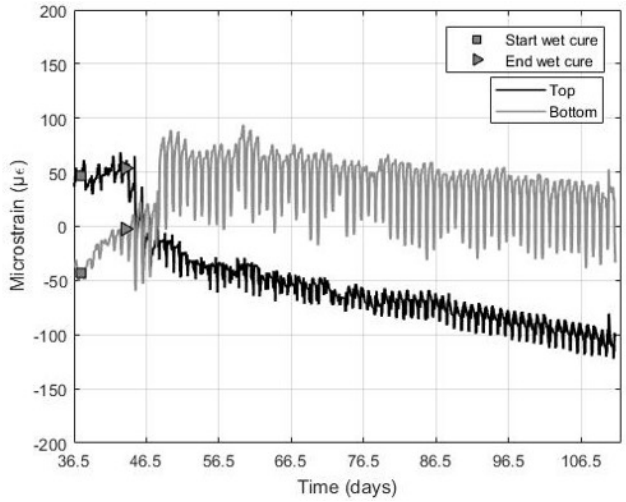


**Figure 53. Strain versus time isolating UHPC for Slab 5.**

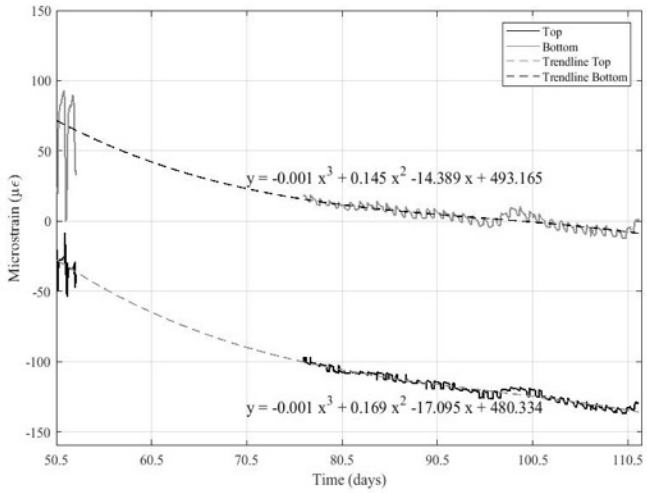


**Figure 54. Strain versus time isolating UHPC after wet cure in Slab 1.**

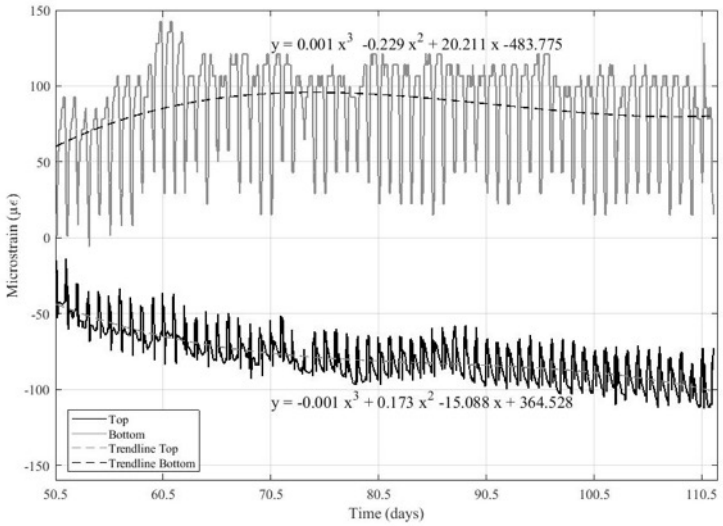


**Figure 55. Strain versus time isolating UHPC after wet cure in Slab 3.**

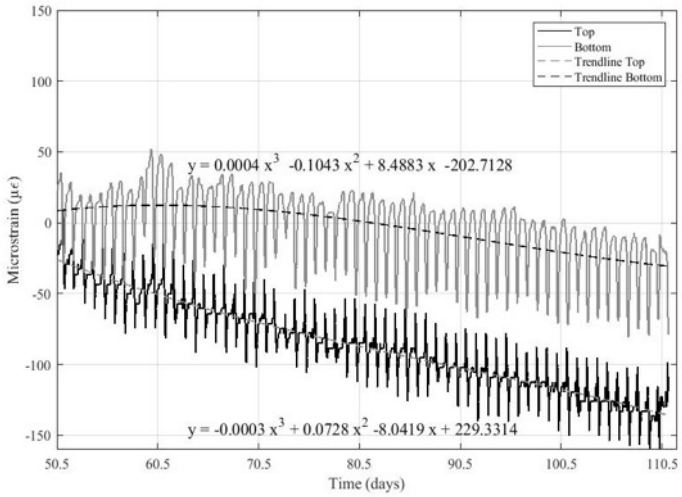


**Figure 56. Strain versus time isolating UHPC after wet cure in Slab 4.**

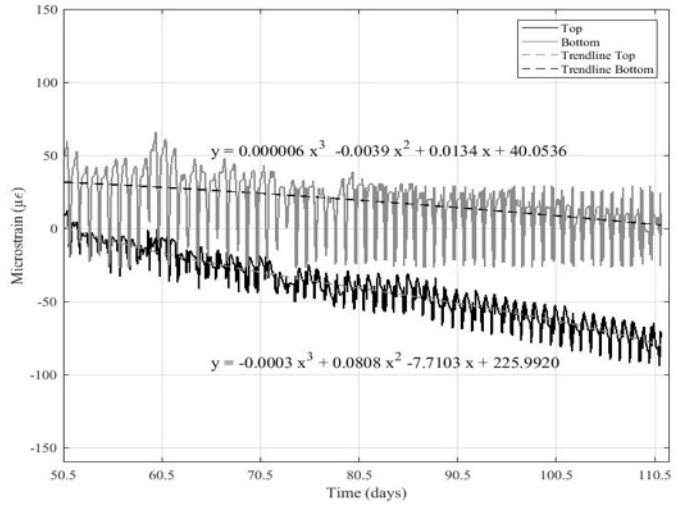


**Figure 57. Strain versus time isolating UHPC after wet cure in Slab 5.**

As shown in Figures 58-61 for Slabs 1, 3, 4, and 5, respectively, the neutral axis rose from almost the mid-height of the slab as the UHPC continued to shrink following the placement of the overlay. This indicates that the bond between the substrate and the overlay was adequate for the two materials to act compositely. Figure 62 shows the neutral axis height for Slabs 1, 3, 4, and 5. The large changes in neutral axis height for Slabs 1 and 5 indicate that the overlay had a significant influence on the behavior. Slabs 3 and 4 had much smaller changes in neutral axis location, demonstrating that the overlay had less effect on the substrate. The increased reinforcement ratio and increased thickness of Slabs 3 and 4 appear to have had a significant influence on the behavior of the system.

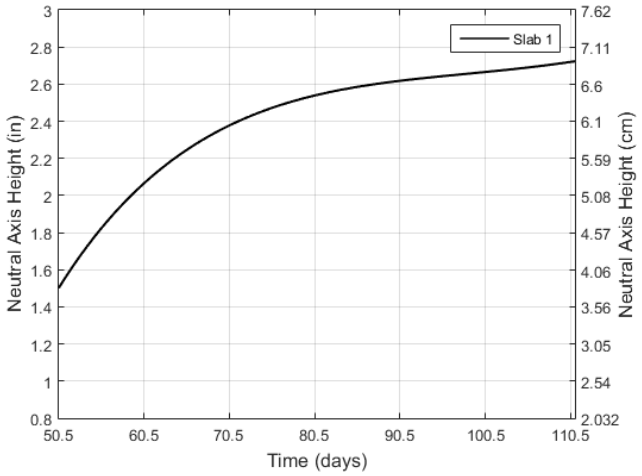


**Figure 58. Neutral axis height for Slab 1.**

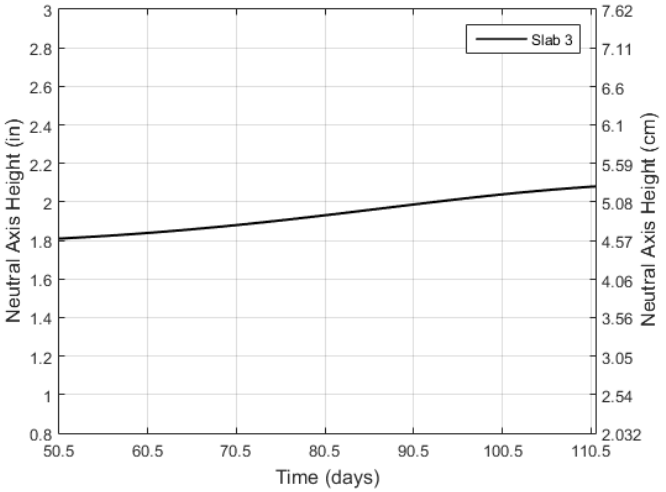


**Figure 59. Neutral axis height for Slab 3.**

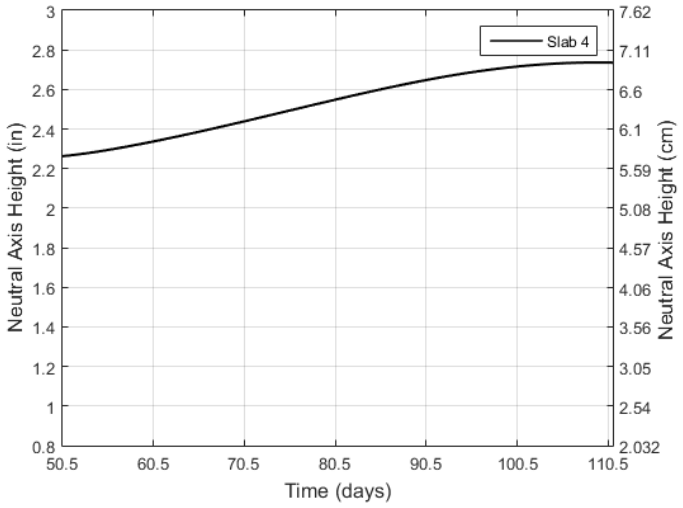


**Figure 60. Neutral axis height for Slab 4.**

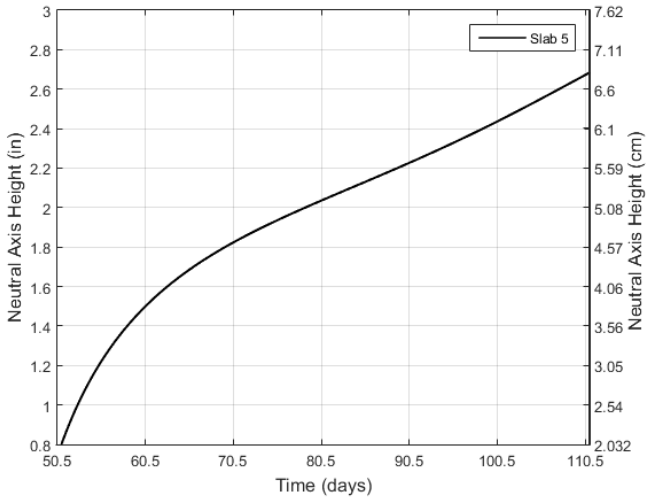


**Figure 61. Neutral axis height for Slab 5.**

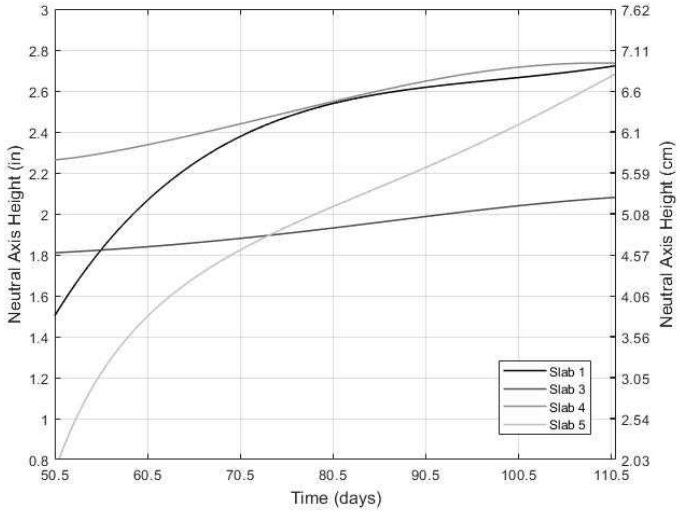


**Figure 62. Neutral axis height.**

## 5.6. Channel Girder Tests

### *5.6.1. Load Deflection Behavior*

The primary global behavior investigated during experimental testing was the load-deflection (P-δ) relationship of girder H-PS-C-300-R-UO when subjected to longitudinal four-point loading. This relationship was determined through analysis of data collected using load cells and string potentiometers as discussed in the Methodology section. Load (P, y-axis) is plotted versus the vertical mid-span deflection (δ, x-axis) captured throughout flexural testing. For these analyses, load was calculated as the sum of both actuator loads recorded by the integrated load cells of the hydraulic actuators. These load cells are accurate to approximately ± 15.0 lb. (66.7 N). Mid-span deflection was taken as the average vertical deflection captured by two string potentiometers positioned at both the east and west longitudinal mid-span locations.

### *5.6.2. Cyclic Loading 1*

Prior to casting the UHPC overlay, flexural testing of girder H-PS-C-300-R-UO was performed using Cyclic Loading 1 (CL1). Using the load configuration shown in Figure 25, the girder was initially loaded at a constant rate 0.1 in./min (2.54 mm/min) to an approximate mid-span deflection of 0.400 in. (10.2 mm). The girder was then unloaded, and the loading was repeated for a total of 1000 load-unload cycles. The loading rate was set at 2 cycles/min for the first 100 cycles, before being increased to 4 cycles/min for the remaining 900 cycles. Load-deflection behavior exhibited during CL1 is presented in Figure 63.

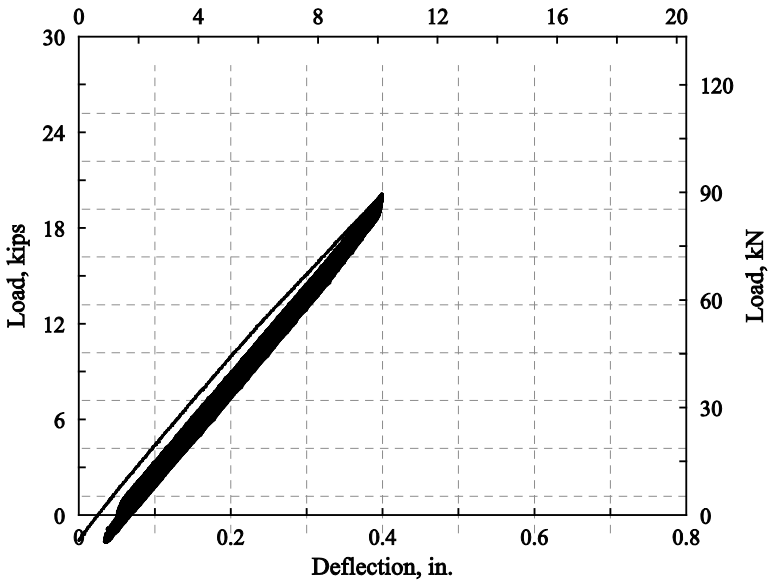


**Figure 63. Load versus mid-span deflection behavior of girder H-PS-C-300-R-UO for CL1.**

Average load and mid-span deflection throughout CL1 were calculated as 20.3 kips (90.5 kN) and 0.397 in. (1.77 mm), respectively. After the initial loading, a residual deflection of approximately 0.034 in. (0.852 mm) was observed as a result of maintaining physical contact, and thus a small amount of load, between the loading apparatus (i.e., actuators and spreader beams). Linear elasticity of girder H-PS-C-300-R-UO was maintained throughout loading, and a residual mid-span deflection of 0.0516 in. (1.31 mm) was recorded at the conclusion of CL1.

### *5.6.3. Cyclic Loading 2*

After addition of the 1.0 in. (25.4 mm) UHPC overlay, Cyclic Loading 2 (CL2) was applied to girder H-PS-C-300-R-UO. As with CL1, the girder was initially loaded at a constant rate of 0.1 in./min (2.54 mm/min) to an approximate mid-span deflection of 0.400 in. (10.2 mm), then subjected to a total of 1000 load-unload cycles. The loading rate was set at 2 cycles/min for the first 100 cycles, before being increased to 4 cycles/min for the remaining 900 cycles. Load-deflection behavior exhibited during CL2 is presented in Figure 64.

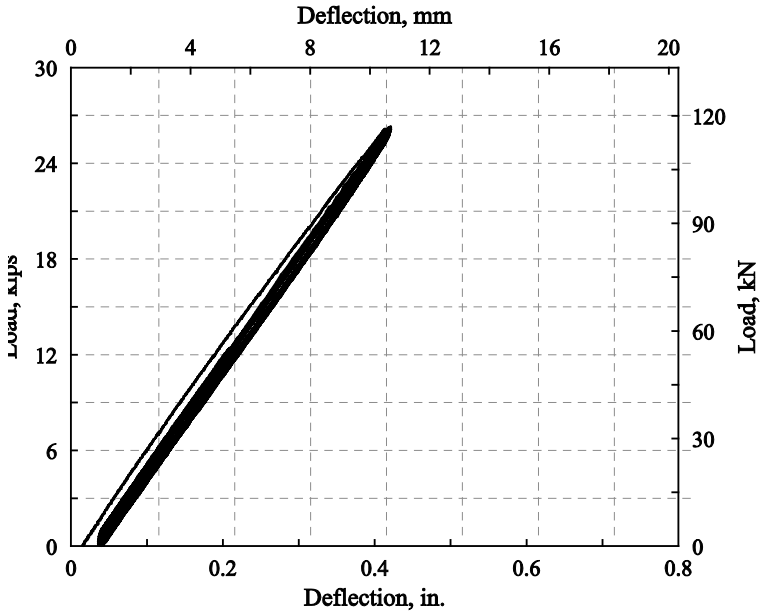


**Figure 64. Load versus mid-span deflection of girder H-PS-C-300-R-UO for CL2.**

Average load and mid-span deflection throughout CL2 were calculated as 25.8 kips (115 kN) and 0.410 in. (10.4 mm), respectively. Similar to CL1, a residual deflection of approximately 0.021 in. (0.533 mm) was observed after the initial loading as a result of maintaining contact between the loading apparatus (i.e., actuators and spreader beams). Girder H-PS-C-300-R-UO continued to exhibit linear-elastic behavior throughout loading, and a residual mid-span deflection of 0.037 in. (0.933 mm) was recorded at the conclusion of CL2. No cracking, debonding, or other visual damage of the UHPC overlay was observed.

### *5.6.4. Comparison of Cyclic Loading*

Comparing the load-deflection behaviors observed during CL1 and CL2, and presented together in Figure 65, there is a clear increase in flexural stiffness exhibited by girder H-PS-C-300-R-UO after addition of the UHPC overlay. To produce the same 0.400-in. (10.2-mm) mid-span deflection required an additional 5.45 kips (24.3 kN) during CL2.

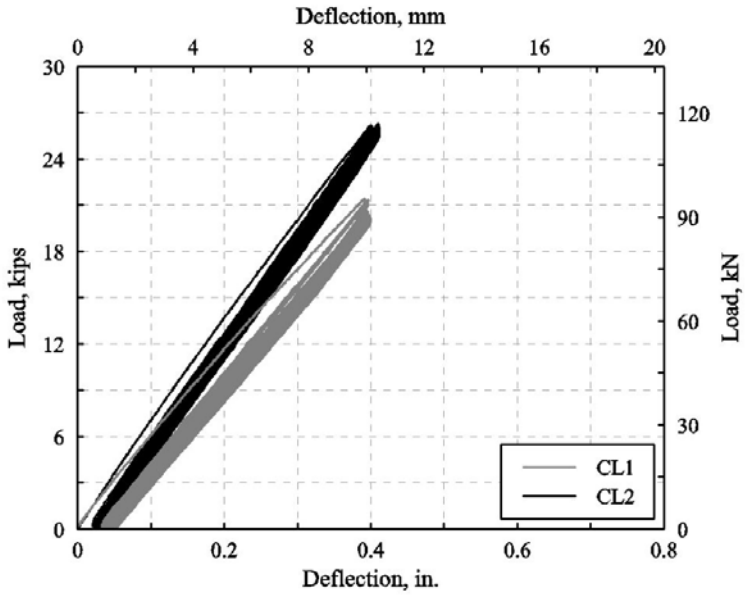


**Figure 65. Comparison of load versus mid-span deflection behavior of girder H-PS-C-300-R-UO for CL1 and CL2.**

### *5.6.5. Ultimate Loading*

The first phase of ultimate loading for girder H-PS-C-300-R-UO consisted of a series of deflection based cyclic loadings. The girder was loaded to a mid-span deflection of 1.0 in. (25.4 mm) at 0.25-in. (6.35-mm) increments, for a total of four increments. At each increment, the girder was cycled (i.e., loaded and unloaded) three times. The load-deflection behavior for each increment is provided in Figure 66.

A constant load rate of 0.05 in./min (1.27 mm/min) was used for the first cyclic loading increments to a mid-span deflection of 0.25 in. (6.35 mm) (Figure 66a). The load rate was then increased to 0.10 in./min (2.54 mm/min) for the remaining three increments (Figure 66b through d). Relevant average load and deflection data for each deflection increment loading is provided in Table 20. Linear behavior was maintained through the first two increments. However, first cracking of girder H-PS-C-300-R-UO occurred during the third increment loading to 0.75 in. (19.1 mm) at a load and deflection of approximately 33.1 kips (147 kN) and 0.53 in. (13.3 mm), respectively. First cracking is labeled in Figure 66c.

After completion of the deflection increment cyclic loadings, girder H-PS-C-300-R-UO was then loaded in 1.0-in. (25.4-mm) increments at 0.10 in./min (2.54 mm/min) to a final ultimate load and deflection. Load-deflection behavior exhibited during final ultimate loading is provided in Figure 67a, and the full dataset for ultimate loading are superimposed and provided in Figure 67b.

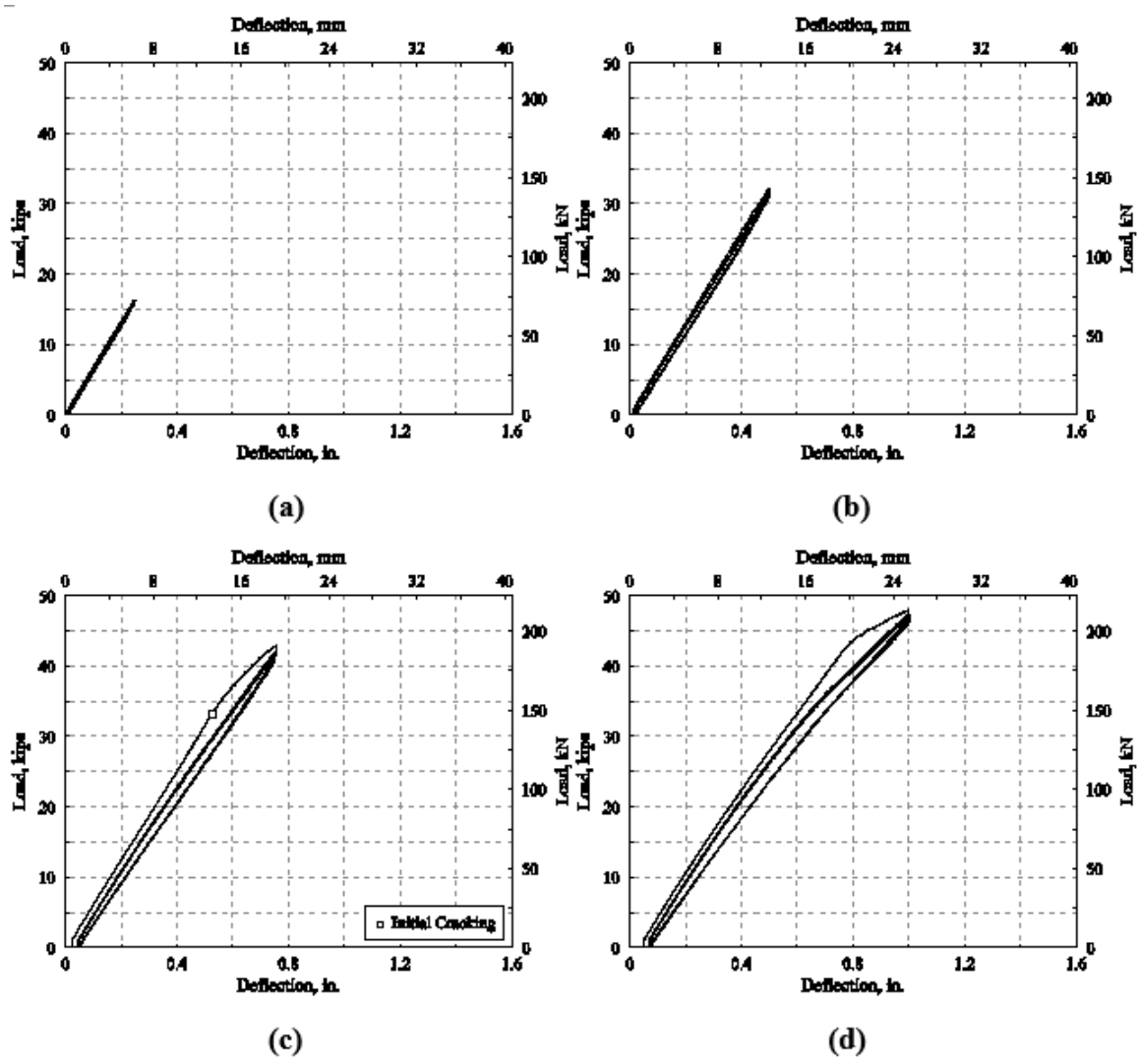


**Figure 66. Load versus mid-span deflection behavior of girder H-PS-C-300-R-UO for ultimate loading deflection increment cyclic loadings: (a) 0.25 in. (6.35 mm), (b) 0.50 in. (12.7 mm), (c) 0.75 in. (19.1 mm), and (d) 1.0 in. (25.4 mm).**

**Table 19. Summary of Load-Deflection Behavior for UL Deflection Increment Cyclic Loadings – Girder H-PS-C-300-R-UO.**

| Increment No. | Target Deflection in. (mm) | Average Load kips (kN) | Max Deflection in. (mm) |
|---|---|---|---|
| **1** | 0.25 (6.35) | 16.3 (72.3) | 0.25 (6.29) |
| **2** | 0.50 (12.7) | 32.2 (143) | 0.50 (12.7) |
| **3** | 0.75 (19.1) | 42.5 (189) | 0.75 (19.1) |
| **4** | 1.00 (25.4) | 47.3 (211) | 1.00 (25.4) |

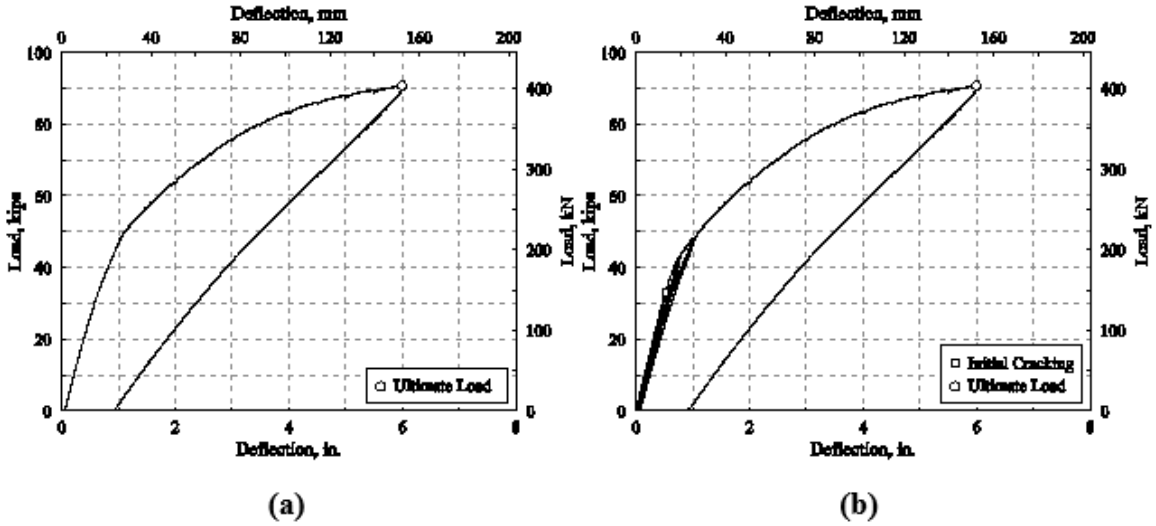


**Figure 67. Load versus mid-span deflection behavior for girder H-PS-C-300-R-UO: (a) final ultimate loading and (b) full ultimate loading dataset.**

Average load and mid-span deflection for final ultimate loading were identified as 90.7 kips (404 kN) and 5.99 in. (152 mm), respectively, as indicated in Figure 67a and b. A residual mid-span deflection of approximately 0.93 in. (23.7 mm) was observed after unloading. At ultimate, girder H-PS-C-300-R-UO exhibited high concentrations of flexural and flexural-shear cracking in and around the pure-moment region, many extending up to deck level (see Figure 68). Little to no cracking, crushing, or other visible distress was observed on the UHPC overlay. Some isolated delamination was noted after unloading, particularly in high shear regions and near the south girder end. Loading was discontinued to avoid ultimate failure of the girder and/or damage to instrumentation.

(a) (b)

**Figure 68. Girder H-PS-C-300-R-UO at ultimate loading: (a) flexural cracking in and around pure moment region and (b) deflected shape.**

### *5.6.6. Summary of Ultimate Loading*

A summary of load-deflection behavior for cyclic and ultimate loading of girder H-PS-C-300-R-UO is provided in Table 20.

**Table 20. Summary of Load-Deflection Behavior for Girder H-PS-C-300-R-UO.**

| **Load Scenario** | **Load Event** | **Average Load** kips (kN) | **Average Deflection** in. (mm) |
|---|---|---|---|
| **CL1** | Maximum | 20.3 (90) | 0.397 (10.1) |
| **CL2** | Maximum | 25.8 (115) | 0.410 (10.4) |
| **UL** | Cracking | 33.1 (147) | 0.525 (13.3) |
| **UL** | Ultimate | 90.7 (404) | 5.99 (152) |

# 6. CONCLUSIONS

Based on the research conducted during the course of this project, the following conclusions were drawn:

1. Development of a proper bond between UHPC and NSC can be achieved without the use of bonding agents. However, bond strength is highly dependent on the texture of the substrate material.
2. Acceptable bond strengths were achieved for all texture depths (0.002 to 0.110 in. [0.05 to 2.8 mm]) with the exception of direct tension bond strengths.
3. Desirable bond strength from slant-shear and splitting tension specimens was achieved even in the case of inadequate texturing (lightly ground texture).
4. Acceptable direct tensile strengths were achieved with chipped textures. Although, grooved textures failed to provide adequate tensile strength, one substrate failure was observed that indicates that the strengths may have been limited by the immature substrate.
5. The results of this study indicate that locally produced UHPC has the potential to serve as an overlaying material as long as proper measures are used in texturing the substrate to ensure that proper bond is achieved.
6. Since the minimum acceptable texture depth under field conditions is 0.25 in. (6.35 mm) and all of the bond assessment tests were able to produce adequate strengths with textures less than 0.08 in. (2 mm), the results are particularly promising.
7. The reinforcement used in the slabs is relevant for shrinkage. As expected, slabs experienced less shrinkage when more steel was provided.
8. Thickness of the substrate was also an important factor for shrinkage. Thicker slabs experienced greater shrinkage than thinner slabs. This observation makes it appear that reinforcement ratio is more important than reinforcement area since comparable slabs contained the same amount of steel.
9. The slab that was exposed only to laboratory conditions experienced shrinkage that was more uniform, as expected.
10. Full-scale testing of a pre-stressed girder demonstrated that a clear increase in flexural stiffness after addition of the UHPC overlay. An approximately 27% increase in load was required to achieve the same 0.400-in. (10.2-mm) mid-span deflection after the overlay was added. This behavior provides evidence of adequate bond development between the UHPC overlay and the HPC girder, which after 100 cycles had exhibited no visible indications of distress or debonding.
11. The flexural behavior exhibited by the girder with a UHPC overlay during ultimate loading provided further confidence in the performance of non-proprietary UHPC for overlay applications. Behavior during deflection increment cyclic loadings provided evidence that the composite section maintained elastic behavior prior to cracking.
12. Final ultimate loading also demonstrated the performance of the UHPC overlay. Even with high concentrations of flexural and flexural-shear cracking in and around the pure-moment region, many extending up to deck level, little to no cracking, crushing, or other visible distress was observed on the UHPC overlay.
13. The only distress observed that was related to the overlay was isolated delamination that occurred at significantly higher loads than expected under normal service conditions.

14. Considering that the average compressive strength of the UHPC overlay on the test day was only 17.80 ksi (122.7 MPa), relatively low for this non-proprietary UHPC, the lack of superficial distress due to such loading is encouraging.

# 7. RECOMMENDATIONS

Based on the literature review and the results of the research performed for this work, the following recommendations are made:

1. Bonding agents were not required to bond UHPC overlay to the substrate material because nano-scale particles in UHPC provide sufficient bond for marginally textured surfaces as long as they are clean.
2. Care should be taken to ensure that prepared surfaces are clean and saturated prior to application of the overlay.
3. Although much of the laboratory work in this research used grinding for surface preparation and texturing, it is not an acceptable practice.
4. Chipping was observed to provide more favorable conditions for bonding of the overlay. However, chipping can cause micro-cracks in the area just under the prepared surface that may cause premature fractures of the composite element after an overlay is applied.
5. Preferred surface preparation methods are shot blasting or hydro-demolition.
6. Direct tension testing is recommended as the most demanding measure of bond strength. This test has the added benefit that it can be performed in the field.
7. For overlay placement on small areas, it is desirable to have level formwork built to the exact desired height of the overlay.
8. Care should be taken to ensure that the UHPC mixture has adequate workability. Additionally, steel screeds and tools are preferable to lumber.
9. Surface finishing techniques for UHPC overlays should be investigated to provide fast, efficient methods for aesthetic finishing without impacting concrete strength. Desirable finishing methods should be able to be performed before the formation of drying shrinkage cracks.
10. Further testing of girder H-PS-C-300-R-UO under transverse three-point loading is recommended to investigate the performance of the non-proprietary UHPC overlay subjected to transverse flexural and high shear load cases.

## REFERENCES


1. Haber, Z.B., Graybeal, B.A., and Munoz, J.F. "Field Testing of an Ultra-High Performance Concrete Overlay." FHWA-HRT-17-096, Federal Highway Administration, 2017.

2. Magureanu, C., Sosa, I., Negrutiu, C., and Heghes, B. "Mechanical Properties and Durability of Ultra-High-Performance Concrete." ACI Materials Journal, Vol. 109, No. 2, 2012, pp. 177-183.

3. Naaman, A.E. and Wille, K. "The path to Ultra-High performance Fibre Reinforced Concrete (UHP-FRC): Five Decades of Progress." Third International Symposium on UHPC and Nanotechnology for High Performance Construction Materials, Kassel, 2012, pp. 3-15.

4. Shann, S.V., Harris, D.K., Carbonell, M.C., and Ahlborn, T.M. "Application of UHPC as a Thin Topped Overlay for Concrete Bridge Decks." Third International Symposium on UHPC and Nanotechnology for High Performance Construction Materials, 2012, pp. 929-936.

5. Montoya, K.F. "Feasibility of Using Ultra High Performance Concrete in New Mexico Bridge Girders." Master's thesis, New Mexico State University, 2010.

6. ASTM C1856: Fabricating and Testing of Ultra-High Performance Concrete, Annual Book of ASTM Standards, ASTM International, Conshohocken, PA, 2017

7. Villanueva, J.M. "Mixture Proportioning and Freezing and Thawing Durability of Ultra High Performance Concrete Using Local Materials." Ph.D. dissertation, New Mexico State University, 2015.

8. Way, R. and Wille, K. "Material Characterization of an Ultra High-Performance-Fibre Reinforced Concrete under Elevated Temperatures." Third International Symposium on UHPC and Nanotechnology for High Performance Construction Materials, Kassel, 2012, pp. 565-572.

9. Al-Basha, A.J. "Frost Resistance of Concrete Cladded with Locally Produced Ultra-High Performance Concrete Cured at Elevated Temperatures." Master's Thesis, New Mexico State University, 2017.

10. Allena, S. and Newtson, C.M., "Shrinkage of Fiber-Reinforced Ultrahigh Strength Concrete." Journal of Materials in Civil Engineering, Vol. 24, No. 5, 2011, pp. 612-614.

11. Lyelle, E. "Optimization of Ultra High Performance Concrete Mixture Proportions using Locally Available Materials." Master's thesis, New Mexico State University, 2012.

12. ICRI 310. "Committee 310: Selecting and Specifying Concrete Surface Preparation for Sealers, Coatings, Polymer Overlays, and Concrete Repair." ICRI310.2R-2013, International Concrete Repair Institute, ICRI, 2013.

13. Silfwerbrand, J., and Beushausen, H. "Bonded Concrete Overlays – Bond Strength Issues." Proceedings of the International Conference on Conference Repair, Rehabilitation and Retrofitting, M.G. Alexander, H.-D. Beushausen, F. Dehn, and P. Moyo, eds., Cape Town, South Africa, Vol. 512, Nov. 2005.

14. Simonsen, J. E. "Low-slump High-density Concrete Bridge Deck Overlay. "Report 75-B-93, Michigan Transportation Commission, 1988.

15. Zhu, Y. "Effect of Surface Moisture Condition on Bond Strength between New and Old Concrete." Bulletin No. 159, Dept. of Structural Mechanics and Engineering, Royal Institute of Technology, Stockholm, Vol. 27, 1992.

16. Delatte, N. J., Williamson, M. S., and Fowler, D. W. "Bond Strength Development with Maturity of High-Early-Strength Bonded Concrete Overlays." ACI Materials Journal, ACI, Vol. 97, No. 2, 2000, pp. 201-207

17. Clímaco, J. C. T. S., and Regan, P. E. "Evaluation of bond strength between old and new concrete in structural repairs." Magazine of Concrete Research, Vol. 53, 2001, pp.377-390

18. Espeche, A. D., and Leon, J. "Estimation of Bond Strength Envelopes for Old-to-new concrete Interface Based on a Cylinder Splitting Test." Construction Building Materials, Vol. 25, 2011, pp.1222-1235.

19. ASTM C882: Bond Strength of Epoxy-Resin Systems Used with Concrete by Slant-Shear, Annual Book of ASTM Standards, ASTM International, Conshohocken, PA, 2013.

20. ASTM C496: Splitting Tensile Strength of Cylindrical Concrete Specimens, Annual Book of ASTM Standards, ASTM International, Conshohocken, PA, 2017.

21. TXDOT. "Test Procedure for Determining the Coefficient of Thermal Expansion of Concrete." Tex-428-A, 2011.

22. ACI Committee 546R-04: Guide to Materials Selection for Concrete Repair, American Concrete Institute ACI546R-04, 2004.

23. ASTM E965: Measuring Pavement Macrotexture Depth Using a Volumetric Technique, Annual Book of ASTM Standards, ASTM International, West Conshohocken, PA, 2015.

24. Holt, E. E., (2001). "Early Age Autogenous Shrinkage of Concrete,", *VTT publication 446*, Technical Research Centre of Finland.

25. Lozoya, J., and Newtson, C. M. (2004). "Effects of Early Misting on Concrete Shrinkage," Proceedings, Advancing Concrete Through Science and Engineering, RILEM, March 2004, Evanston.

26. ASTM C157: Length Change of Hardened Hydraulic-Cement Mortar and Concrete, Annual Book of ASTM Standards, ASTM International, Conshohocken, PA, 2017

27. ASTM C1202: Electrical Induction of Concrete's Ability to Resist Chloride Ion Penetration, Annual Book of ASTM Standards, ASTM International, Conshohocken, PA, 2012.

28. ASTM C39/C 39M-0.5: Standard test method for Compressive Strength of Cylindrical Concrete Specimens, Annual Book of ASTM Standards, ASTM International, West Conshohocken, PA, 2005.

29. BS 1881 Part 116: British Standard Testing concrete, British Standards Institution, London, UK, 1983.

30. ASTM C78/C78M: Standard test method for Flexural Strength of Concrete (Using Simple Beam with Third-Point Loading), Annual Book of ASTM Standards, ASTM International, West Conshohocken, PA, 2018.

31. ASTM C1609/C1609M: Standard test method for Flexural Performance of Fiber-Reinforced Concrete (Using Beam with Third-Point Loading)[1], Annual Book of ASTM Standards, ASTM International, West Conshohocken, PA, 2012.

32. ASTM C469/C469M: Standard test method for Static Modulus of Elasticity and Poisson´s Ratio of Concrete in Compression, Annual Book of ASTM Standards, ASTM International, West Conshohocken, PA, 2014.

33. LRFD Bridge Design Specifications, 6th ed. AASHTO, Washington, D.C., 2012.

34. Carbonell, M. A., Harris, D. H., Shann, S. V., and Ahlborn, T.M. "Bond strength between UHPC and normal strength concrete (NSC) in accordance with split prism and freeze-thaw cycling tests." In Proc., Hipermat 2012 3rd Int. Symp. on UHPC and Nanotechnology for High Performance Construction Materials, 2012, pp. 377-384.

35. ASTM A615/A615M: Deformed and Plain Carbon-Steel Bars for Concrete Reinforcement, Annual Book of ASTM Standards, ASTM International, Conshohocken, PA, 2015.

36. ASTM A370: Mechanical Testing of Steel Products, Annual Book of ASTM Standards, ASTM International, Conshohocken, PA, 2014.

37. Harris, D.K., Sarkar, J., and Ahlborn, T.M., "Characterization of Interface Bond of Ultra-High Performance Concrete Bridge Deck Overlays." Transportation Research Board, Vol. 2240, No., 2011, pp. 40-49.

38. Sprinkel, M.M. and Ozyldirim, C. "Evaluation of High Perfomance Concrete Overlays Placed on Route 60 Over Lynnhaven Inlet in Virginia." 2000.

39. Ahlborn, T., Peuse, E., Misson, D., & Gilbertson, C. (2008). "Durability and strength characterization of ultra-high performance concrete under variable curing regimes," In *Proceedings of the 2nd International Symposium on Ultra-High Performance Concrete, Kassel, Germany* (pp. 197–204).

40. Bonneau, O., Lachemi, M., Dallaire, E., Dugat, J., & Aitcin, P. (1997). "Mechanical properties and durability of two industrial reactive powder concretes," *ACI Materials Journal, 94*(4), 286–290.

41. Graybeal, B., & Davis, M. (2008). "Cylinder or cube: strength testing of 80–200 MPa (11.6–29 ksi) ultra-high performance fibre-reinforced concrete," *ACI Materials Journal, 105*(6), 603–609.

42. Scheydt, C., & Muller, S. (2012). "Microstructure of ultra high performance concrete (UHPC) and its impact on durability," In *Proceedings of the 3rd International Symposium on UHPC and Nanotechnology for High Performance Construction Materials, Kassel, Germany* (pp. 349–356).